The Pennsylvania State University

The Graduate School

Eberly College of Science

AN INVESTIGATION OF THE PHOTOEXCITATION DYNAMICS AND STABILITY OF CLUSTERS

A Thesis in

Chemistry

by

Kevin Matthew Davis

Submitted in Partial Fulfillment
of the Requirements
for the Degree of

Doctor of Philosophy

May 2007

The thesis of Kevin Matthew Davis was reviewed and approved* by the following:

A. Welford Castleman, Jr.
Evan Pugh Professor of Chemistry and Physics
Thesis Advisor
Chair of Committee

James B. Anderson
Evan Pugh Professor of Chemistry

John V. Badding
Associate Professor of Chemistry

Peter C. Eklund
Professor of Physics

Ayusman Sen
Professor of Chemistry
Head of the Department of Chemistry

*Signatures are on file in the Graduate School

ABSTRACT

The research discussed in this thesis has two different themes. First, photoexcitation studies delve further into the fundamental phenomena of clusters. One of the processes considered is the emission of a delayed atomic ion upon photoexcitation of a molecular beam of metal-carbon clusters. The origin of this delayed atomic ion is uncovered by simultaneously studying the delayed ionization of zirconium and titanium carbides using species produced with a mixed metal alloy rod in a standard laser vaporization source coupled to a time-of-flight mass spectrometer. These experiments have provided the ability to observe, for the first time, both the zirconium and titanium delayed atomic ions concurrently. Through an extensive investigation of clusters formed under these conditions, the origin of the delayed atomic ions is elucidated and a mechanism is proposed. The mechanism states that the delayed atomic ion is a product of a delayed ion-pair separation that is formed due to the excitation of the MC_2 molecule to a compilation of Rydberg states near its ionization threshold. The detection of C_2^- following excitation of M_xC_y clusters provides further evidence of this mechanism being the source of the delayed M^+ emission.

Furthermore, the design and calibration of an anion photoelectron spectrometer is discussed in this thesis. Copper anions are isolated using a time-of-flight mass spectrometer. The copper anion is then excited to its neutral state by removing an electron. The photodetached electron is analyzed by a "velocity map imaging" photoelectron spectrometer, which determines its kinetic energy. This information allows for the determination of copper's photoelectron spectrum, which provides insight into its

electron affinity that can be used as a calibrant to aide the study of clusters in future experiments.

The second theme of this thesis regards a new protocol that is proposed providing a pathway to producing materials with clusters as their building blocks. Through a synergistic effort by Professor Castleman's research group, Professor S. N. Khanna's research group, and Professor A. Sen's research group that combined results of gas phase, theoretical and synthetic research, the feasibility of this procedure is demonstrated by making a solid via assembly and comprised of As_7K_3 units identified as being a stable magic cluster in the gas phase. X-ray diffraction and theoretical studies show the material to have rings consisting of As_7 and K units as its building block. To our knowledge, the example presented herein offers the first viable protocol for accomplishing successful passage from free gas-phase clusters to cluster-crystals.

TABLE OF CONTENTS

LIST OF FIGURES

ACKNOWLEDGEMENTS

First, I would like to thank my advisor, A. W. "Will" Castleman, Jr. Will has been a wonderful mentor. I am very thankful he gave me the opportunity to work in his group and learn from his guidance. Under his leadership, I have had many learning experiences unlike any others in my life. It was a pleasure to work with someone so kind and with such a wonderful grasp of the world of chemistry. I also want to thank the other professors who have been important in my graduate school success. Thank you to Professor Anderson, Professor Badding and Professor Eklund for participating on my committee. Thank you, Professor Sofo, Professor Khanna and Professor Sen for the successful collaborations over the course of my graduate career. Thank you, Professor Hoenigman and Professor Shubert, my undergraduate chemistry professors at Newman University, for guiding me to graduate school at Penn State University.

Next, I would like to thank the group members of the Castleman group that I had the privilege of working with during the course of my graduate school career. Most notably, Sam Peppernick, who worked with me on the research discussed within this thesis. He has been a great colleague and an even better friend. Also, I would like to thank Mark Merritt, who joined our research project late in my graduate career, but didn't hesitate to make an impact and quickly became an important part of our research team and a good friend.

I would also like to thank the members of the Research Instrumentation Facility at Penn State University. They are a vital part of accomplishing research in an instrumentation heavy group like the one in which I worked. Thank you, Rod, Bob and

Jim for teaching me the world of electronics, fixing old electronics, building new electronics and keeping our lasers functioning properly. Also, special thanks go to Bob Holden and the rest of the Chemistry Maintenance Shop. Bob Holden helped me come up with numerous ideas to help keep our instrument running at its peak potential. The Chemistry Maintenance Shop was also an integral part of our move to the new chemistry building. Thank you, Barry Dutrow and the rest of the Physics Machine Shop for helping design and manufacturing many improvements to the instrument. In addition, I want to thank Connie Smith as well as the other faculty members that aided in my graduation.

Finally, I thank my family and friends. My parents are my heroes and they have guided me throughout all of my life. I never would have accomplished anything in life without their love and support. My brother has also been a key part of my graduate school life. We have grown very close over the course of my time in graduate school. I also want to thank my wife Cheryl for helping me get through the many trials that accompany graduate school life.

Chapter 1

Introduction

The overall goal and motivation of the research presented in this thesis is to further the knowledge of clusters in the hope that they will be utilized in the future as building blocks to new materials that exploit their unique properties. To this end, the research discussed herein has two different themes. First, investigations into a cluster's response to stimulation in the gas phase provide insights into the properties and potential uses of the materials. In the case of the research presented within this thesis, photoexcitation is the stimulant, and the emission of an electron is the effect that is studied in various ways. Second, gas phase experiments attempt to discover clusters that have potential to serve as building blocks to new materials. Through collaboration with Professor A. Sen and Professor S. N. Khanna, an example of successful passage from gas-phase magic clusters to cluster-crystals is presented.

1.1 Photoexcitation Studies

Generally, when a metal surface absorbs a photon that contains enough energy to excite an electron above a binding threshold, the surface will emit an electron for every interacting photon, which is termed the photoelectric effect. However, electrons, atoms and molecules can also be emitted from a surface following thermal excitation of its vibrational modes, which is termed thermionic emission. In clusters, the ionization

pathway is dominated by prompt ionization that occurs on the femtosecond timescale and is analogous to the photoelectric effect. However, some clusters have been observed to delay ionize on a microsecond timescale, which is analogous to thermionic emission. Generally, clusters that delay ionize have a significant number of vibrational modes as well as a higher binding energy than ionization potential.

Delayed ionization in clusters was first discovered in the Castleman group in 1986 by Dao and Castleman in ionization studies of clusters comprised of paraxylene bound to trimethyl amine.[**1**] Dao and Castleman observed long tails to the slow side of trimethylamine ions, which was attributed to its delayed ionization relaxation pathway. Shortly thereafter, Nieman *et al.*, examined this phenomenon in transition metal oxide clusters following multiphoton excitation.[**2**] Since, many studies on various types of clusters have observed the phenomenon delayed ionization, including metal carbides[**3**][**4**][**5**][**6**] and fullerenes[**7**][**8**][**9**][**10**][**11**].

One interesting observation that was made while studying delayed ionization of M_xC_y clusters (where M is Ti, V, and Nb) is the apparent delayed ionization emission pathway of various metal atoms. This is an anomaly because an atom does not contain any vibrational modes to allow for the thermionic emission of electrons at a delayed time. While performing a delayed ionization study on both titanium and zirconium carbide clusters, the origin of this delayed atomic ion was uncovered. Report of these findings is the subject of Chapter 3.[**12**] Rather than an impossible excitation of vibrational modes of an atom, a mechanism consisting of the delayed emission of a M^+ from an excited MC_2 ion-pair unit is deduced. While ion-pair separation is not thought to be a primary relaxation pathway of clusters, it has been studied on numerous occasions.[**13**][**14**][**15**]

Generally, this is a mechanism that occurs when Rydberg states just below the ionization potential of the molecule under study are accessed. Ion-pair separation is the subject of the research discussed in Chapter 4, which provides support for the previously proposed mechanism of ion-pair separation leading to the delayed emission of metal atoms. This research involves the detection of negative ions after exciting a neutral molecular beam, which is evidence of ion-pair separation.

1.2 Photoelectron Spectroscopy

Anion photoelectron spectroscopy (PES) is an interesting avenue of research that analyzes photodetached electrons rather than the previously discussed experiments that examined ionized clusters. In anion PES, electrons are photodetached from negatively charged species and analyzed to obtain their kinetic energy. The kinetic energy is equal to the energy received from absorbing a photon minus the binding energy of that electron. Therefore, the kinetic energy of the emitted electron elucidates electronic and vibrational states of the neutral molecule that cause different binding energies of the electron as is displayed in Figure **1.1**. The knowledge of a cluster's photoelectron spectrum provides information regarding its electron affinity and vertical detachment energy.

Velocity map imaging is an experimental technique to obtain the photoelectron spectrum of a given cluster. Velocity map imaging was first performed by Eppinck and Parker in 1997.[**16**] They demonstrated a substantial improvement to 2D electron imaging technique by using open electrostatic lenses rather than electrostatic lenses with

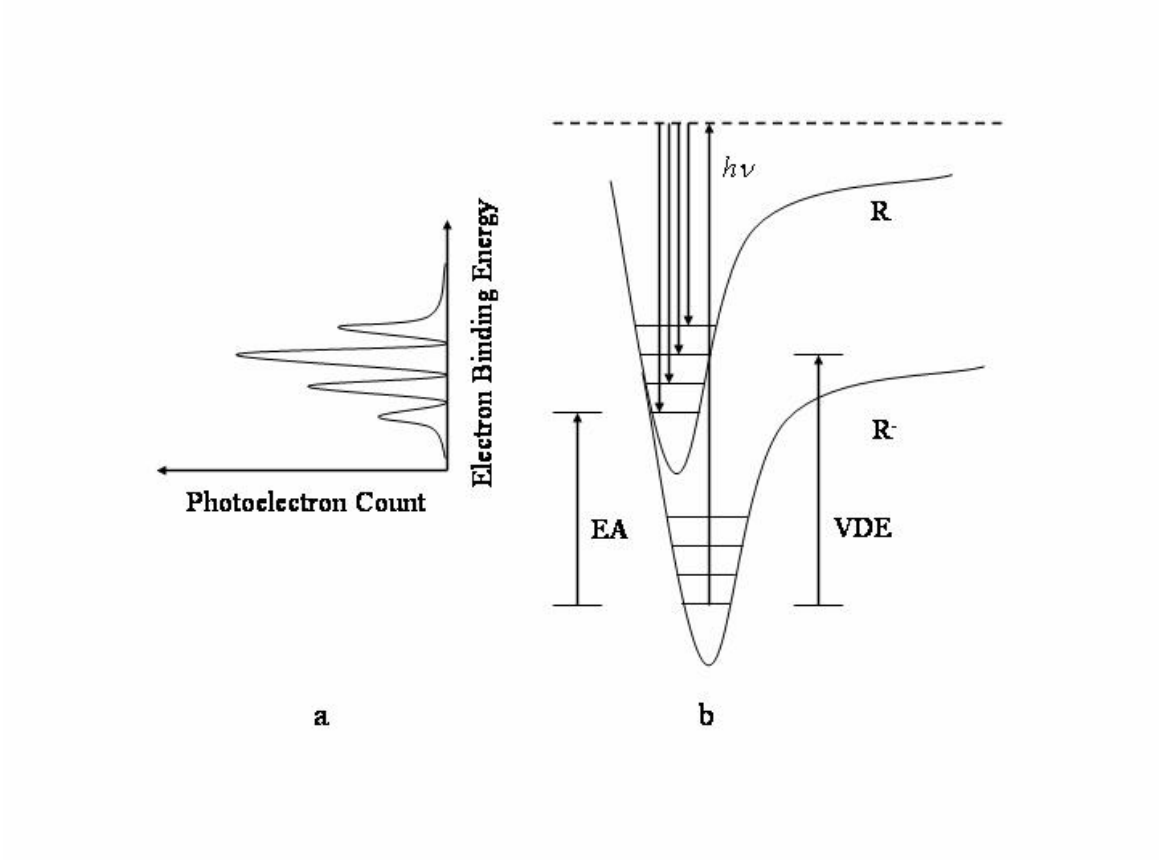

Figure **1.1**: Qualitative diagram displaying the resulting photoelectron spectrum (a) of a photodetached electron following excitation from the ground state of R^- to a virtual level in the $R + e^-$ continuum by a photon of fixed energy, hν (b). The electron affinity (EA) of R and the vertical detachment energy (VDE) of R^- are labeled. Adopted from Ervin and Lineberger.[**17**]

fine wire mesh covering the open holes. In a velocity map imaging stack, an electric field extracts the electrons in such a manner that maps all electrons with the same initial velocity to a point equidistant from the center of a position sensitive detector.[**16**] Photodetached electrons with different kinetic energy expand at different speeds and are detected at different radii from the center of the detector (see Figure **1.2**). The result is a series of rings that correspond to photodetached electrons with different kinetic energies allowing for the photoelectron spectrum to be extracted from images taken with a charge-coupled device camera. The design and calibration of a velocity map imaging apparatus is the subject of Chapter 5.

1.3 Clusters to Crystals

The previously discussed research is conducted in an attempt to further the knowledge of a cluster's response to the absorption of photons as well as the physical properties that accompany this process. The second area of research that is discussed in this thesis regards the ongoing search to discover new interesting clusters that are particularly stable in the gas phase and have potential to be a building block to a new material. Since the discovery of C_{60} by Smalley and co-workers,[**18**] the search for other stable clusters in the gas phase that have potential as building blocks to new materials has become a prominent area of research.

Two other clusters that show promise as building blocks to new materials were discovered within the Castleman group. In 1989, Leuchtner, Harms and Castleman

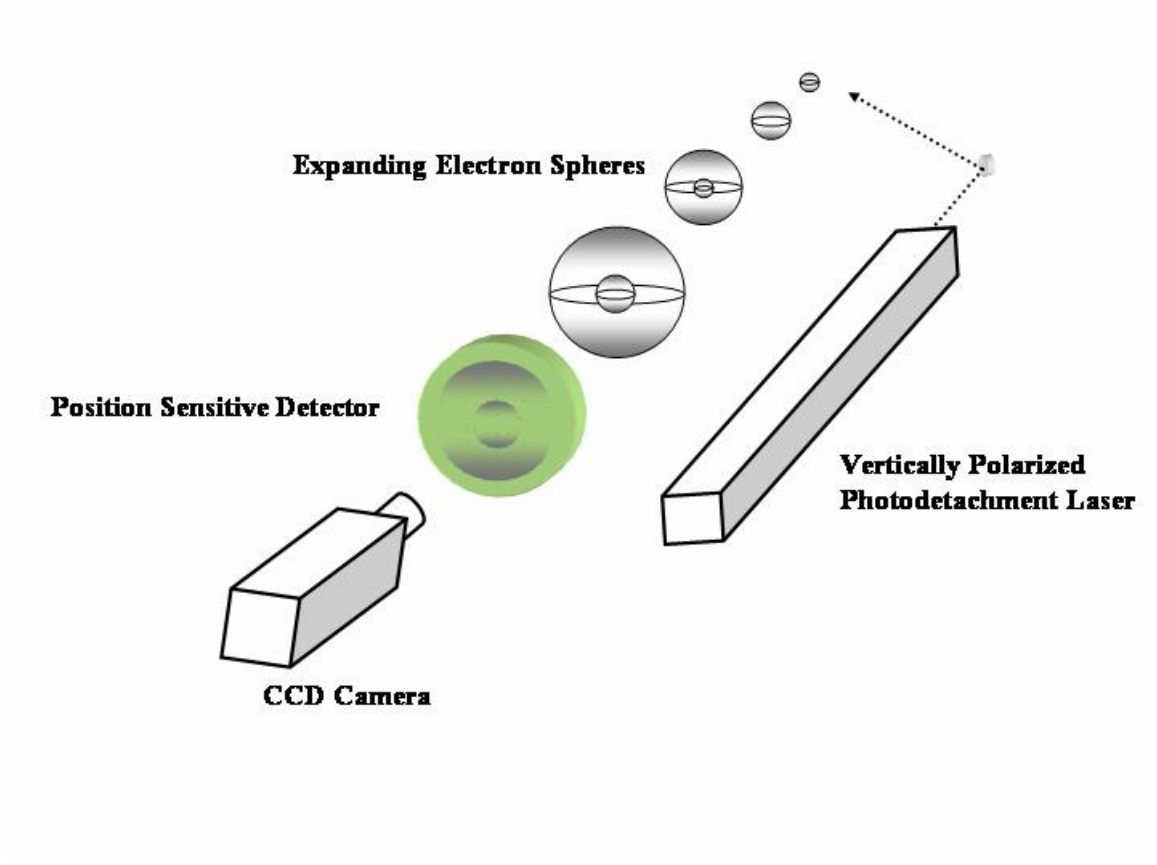

Figure **1.2**: Diagram portraying the expanding electron spheres that contain information regarding the kinetic energy of the photodetached electron as they travel toward a position sensitive detector in the velocity map imaging apparatus. The larger sphere represents electrons with a given kinetic energy higher than the electrons contained within the smaller sphere.

conducted experiments investigating the reactivity of aluminum clusters to oxygen.[**19**] The Al_{13}^- cluster was found to be particularly inert. The result was interpreted to be the effect of a 40 electron valence shell, which is a closed shell in the jellium model. The cluster can be thought of as a super halogen atom in which each aluminum atom donates 3 electrons to the cluster's valence shell giving the cluster 39 valence electrons. Similar to a halogen atom, the Al_{13} cluster has an extremely high electron affinity due to it being one electron short of having a closed shell.

In 1992, Guo, Kerns and Castleman discovered the first of a series of clusters known as the metallocarbohedrenes, M_8C_{12} where M is an early transition metal.[**20**] The titanium metallocarbohedrene (Ti_8C_{12}) was first discovered serendipitously when small hydrocarbons were reacted with titanium. The hydrocarbons were found to undergo a dehydrogenation reaction leaving carbon to react with titanium and form the new class molecular clusters.

The subject of Chapter 6[**21**] is a third special stable cluster that was recently researched in the Castleman group. Through a synergistic effort among gas phase, theoretical and synthetic research, As_7K_3 has been proven to be a potential building block through gas phase molecular beam experiments starting from a dispersed mixture of bulk arsenic and potassium. Employing the idea that the As_7K_3 species identified in the gas phase is a uniquely stable Zintl entity that could affect self-assembly, Professor A. Sen and his research group synthesized and characterized a cluster assembled material having a lattice of $As_7K_{1.5}$. In addition to the experimental work, Professor S. N. Khanna and his research group performed theoretical calculations have confirmed the stability of the As_7K_3 cluster as well as the existence of a stable $(As_7K_2)_6$ ring structure, wherein clusters

are bound together through the sharing of potassium atoms. The results demonstrate the development of a successful protocol for the production of nanoscale materials through cluster assembly.

1.4 References

1. D. Dao and A. W. Castleman, Jr., J. Chem. Phys. **84**, 1435 (1986).

2. G. C. Nieman, E. K. Parks, S. C. Richtsmeier, K. Liu, L. G. Pobo, and S. R. Riley, High Temp. Sci. **22,** 115 (1986).

3. B. D. May, S. F. Cartier, and A. W. Castleman, Jr., Chem. Phys. Lett. **242,** 265 (1995).

4. S. F. Cartier, B. D. May, and A. W. Castleman, Jr., J. Chem. Phys. **104,** 3423 (1996).

5. J. R. Stairs, K. M. Davis, S. J. Peppernick, and A. W. Castleman, Jr., J. Chem. Phys. **119,** 7857 (2003).

6. J. R. Stairs, S. J. Peppernick, K. M. Davis, and A. W. Castleman, Jr., Israel J. Chem. **44,** 223-228 (2004).

7. E. E. B. Campbell, G. Ulmer, and I. V. Hertel, Phys. Rev. Lett. **67,** 1986 (1991).

8. D. Ding, J. Huang, R. N. Compton, C. E. Klots, and R. E. Haufler, Phys. Rev. Lett. **73,** 1084 (1994).

9. H. Lin, K.-L. Han, Y. Bao, E. B. Gallogly, and W. M. Jackson, J. Phys. Chem. **98,** 12495 (1994).

10. J. U. Andersen, P. Hvelplund, S. B. Nielsen, U. V. Pedersen, and S. Tomita, Phys. Rev. A **65,** 053202 (2002).

11. A. Lassesson, K. Mehlig, A. Gromov, H. Shinohara, and E. E. B. Campbell, J. Chem. Phys. **117,** 9811-9817 (2002).

12. K. M. Davis, S. J. Peppernick and A. W. Castleman, Jr., J. Chem. Phys. **124**, 164304 (2006).

17. J. Berkowitz and W. A. Chupka, J. Chem. Phys. **45**, 1287 (1966).

14. U. Rockland, H. Baumgärtel, E. Rühl, O. Lösking, H S. P. Müller and H. Willner, Phys. Chem. Chem. Phys. **99**, 969 (1995).

15. N. Ohmichi, J. Silberstein, and R. D. Levine, J. Phys. Chem. **85**, 3369 (1982).

16. A. T. J. B. Eppink and D. H. Parker, Rev. Sci. Instrum. **68**, 3477 (1997).

17. K. M. Ervin and W. C. Lineberger, *Advances in Gas Phase Ion Chemistry*, edited by N. G. Adams and L. M. Babcock (JAI Press, Greenwich, 1992), Vol. 1, pp. 121.

18. H. W. Kroto, J. R. Heath, S. C. O'Brien, R. F. Curl and R. E. Smalley, Nature **318**, 162 (1985).

19. R. E. Leuchtner, A. C. Harms and A. W. Castleman, Jr., J. Chem. Phys. **91**, 253 (1989).

20. B. C. Guo, K. P. Kerns and A. W. Castleman, Jr., Science **255**, 1411 (1992).

21. A. W. Castleman, Jr., S. N. Khanna, A. Sen, A. C. Reber, M. Qian, K. M. Davis, S. J. Peppernick, A. Ugrinov, and M. D. Merritt, Nano Letters (submitted 2006).

Chapter 2

Experimental Details

2.1 Overview

The experiments discussed in this thesis were performed on a Wiley-McLaren[**1**] time-of-flight mass spectrometer coupled to a laser vaporization source. A diagram of the instrument prior to the installation of a velocity map imager is depicted in Figure **2.1**. Briefly, a metal rod is ablated in a laser vaporization source by the second harmonic of a Nd:YAG laser, while undergoing rotation and translation. Simultaneously, a reactant or carrier gas is pulsed over the rod whereupon the produced clusters are supersonically expanded into a vacuum chamber. The clusters are skimmed prior to the molecular beam traveling between two time-of-flight grids, which make up the acceleration region. Upon entering the acceleration region an electric field directs ions perpendicular to the molecular beam into a field-free region, where they separate based on their mass. In order to study neutral clusters, the ions created in the source are directed off access and a XeCl excimer laser is used to ionize the neutral clusters. After traveling through the field-free region, the clusters enter a reflectron that deflects the ions through another field-free region prior to detection using a microchannel plate (MCP) detector. The signal from the MCP is collected, amplified and sent to the computer for analysis.

The experiments are conducted at a rate of 30 Hz. The master clock is produced by a PSU Pattern Generator. The experiments are performed within a vacuum chamber

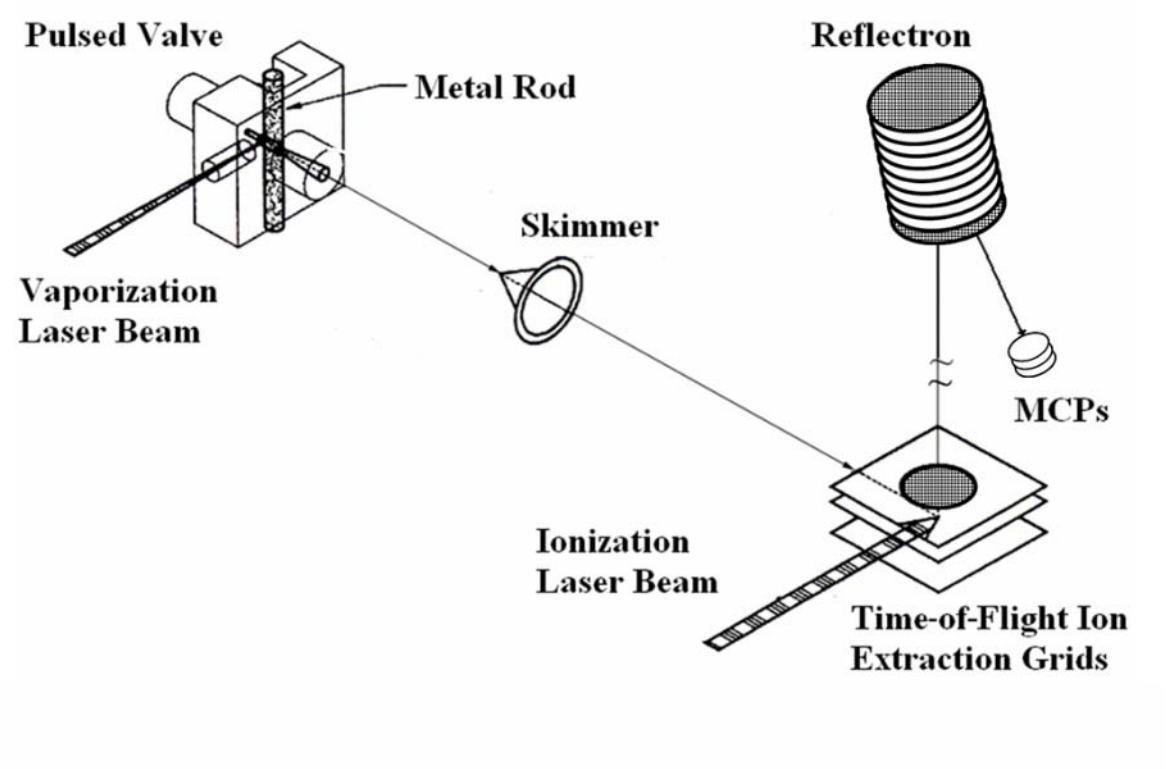

Figure **2.1**: Diagram of the instrument prior to modifications. A laser vaporization source is coupled to a reflectron time-of-flight mass spectrometer.

that is differentially pumped to a base pressure of ~1 x 10^{-7} Torr. The laser vaporization source, time-of-flight mass spectrometer, and velocity map imager are discussed in more detail in the subsequent sections.

2.2 Laser Vaporization Source

A laser vaporization source was utilized to produce a variety of clusters in order to investigate their electronic properties and overall stabilities. The clusters are produced by vaporizing a metal rod with the second harmonic, 532 nm, of a pulsed Nd:YAG laser (Spectra-Physics, GCR-150, ~50 mJ/pulse, ~10 ns pulse), while simultaneously passing gas (~10-15% reactant gas seeded in helium) over the metal rod.

The metal rod is ~2 inches in length and ¼ inches in diameter. The rod rotates and translates in a stepwise manner at a rate of 30 Hz. to ensure a new surface is ablated with every laser pulse. The entire stepper motor assembly is kept under vacuum during experimentation to decrease the amount of impurities introduced into the system, which is a problem for sources that only have the rod under vacuum.

The reactant gas and helium are mixed in a stainless steel sample tank and the mixture is introduced into the apparatus via a pulsed valve (General Valve Series 9). The valve is operated at a backing pressure of ~200 kPa. The length of time the pulse valve is opened is adjusted until optimal signal is reached, which generally results in a source pressure of ~6 x 10^{-6} Torr.

The laser ablation causes a hot plasma of metal atoms to form around the rod. When gas is pulsed over this plasma, atomization of the reactant gas occurs, which allows

atoms in the reactant gas to react with the metal atoms to form both neutral and ionic clusters. The clusters cool as they are supersonically expanded into the vacuum. The housing that contains the metal rod and the pulse nozzle is made of Teflon^{TM}. The clusters that expand from the Teflon^{TM} nozzle are skimmed ~10 cm from the nozzle opening creating a molecular beam of various sized clusters.

2.3 Reflectron Time-of-Flight Mass Spectrometer

The reflectron time-of-flight mass spectrometer (RTOFMS) is an analytical tool, which exploits the charge of a cluster to determine its mass. In the RTOFMS, an electric field perpendicular to the molecular beam accelerates charged clusters of various masses down a long field-free region allowing them to separate by their mass/charge ratio prior to entering the reflectron. The reflectron turns the ions through another field-free region toward the microchannel plates detector. The output is amplified and sent to an oscilloscope for observation and analysis.

The molecular beam enters into the acceleration region that consists of three time-of-flight (TOF) grids that are arranged in a Wiley-McLaren[**1**] setup, which has a two stage acceleration region.[**2**] The electric field caused by the TOF grids is perpendicular to the molecular beam. The time-of-grids are two inches square with a 1-1.5 inch in diameter hole in the center which is covered with electroformed nickel fine wire mesh (45 x 45 holes per inch). All three grids are electrically isolated from one another. TOF grids 1 and 2 are separated by 12.75 mm and make up the first acceleration region. TOF

grids 2 and 3 are separated by 6.5 mm and are the source of the second acceleration region. TOF 3 is always held at ground and is the start of the field-free region.

If a neutral molecular beam is under study, the clusters are ionized by a pulsed 308 nm XeCl excimer laser (EMG-201 MSC, ~10 mj/pulse, 15 ns pulse). The ions travel perpendicular to the molecular beam down a field-free region six feet in length, where they enter a reflectron. The reflectron consists of a twelve aluminum rings that are three inches in diameter. The first ring is held at ground and is covered with a fine wire mesh, which ends the first and begins the second field-free region. The eleven remaining rings are each separated by a resistor. A potential is placed on the first and last of these eleven rings. The potential on the last ring is always higher than the potential on TOF 1, which ensures that all ions will be turned around and directed toward the detector. The potential on the first ring is lower and is adjusted for best mass resolution. The resistors connecting the rings create a potential gradient that gradually slows the ions down and then accelerates them through a second field-free region toward the detectors. The last ring is also covered with wire mesh. The reflectron allows for further separation of the ions under study.

At the end of the second field-free region, the ions travel through a grounded wire mesh, which ends the second field-free region and into a mount assembly wherein the microchannel plates detector (MCPs) resides. The MCPs (Del Mar Ventures, 25-10E) are in a V-stack (Chevron style) and are 25 mm in diameter. When detecting cations, the front plate of the microchannel plate is kept at -2100 V, while the second plate is held at -400 V. When the ions impact the microchannel plate detector, the +1700 V electric field gradient creates an electron cascade. The electrons are collected by a metal anode, which

is held at ground potential. The collected signal is sent through an amplifier to the data acquisition card (Gage, Compuscope 12100) that acts as an oscilloscope. The output is a mass spectrum, where intensity is proportional to the number of ions that collide into the detector at a particular time. The data acquisition card is a 12 bit card that acquires data at a speed of 100 megasamples per second, which corresponds to a data point every ten nanoseconds. A mass spectrum generally consists of 15000 points, or 150 μs of data. Each mass spectrum is averaged over hundreds of laser shots.

2.3.1 Delayed Ionization Studies of Neutral Clusters

Delayed ionization is studied by manipulating the time-of-flight grid furthest from the detector (TOF 1); see Figure **2.2**. A potential of 4500 V is applied to this grid, while a constant 3000 V potential is placed on the grid closer to the detector (TOF 2). The consequent electric field accelerates cations toward the reflectron. During delayed ionization experiments, the potential on TOF 1 is applied using a fast high voltage switch (FHVS, Behlke HTS-51), which has a ~15 ns rise time and remains on for 12.75 μs prior to slowly decaying back to ground ~80 μs later. The grid is kept at ground when the switch is off, producing an electric field that directs cations away from the detector. Initially, the switch is turned on prior to the ionization laser interacting with the molecular beam. During the delayed ionization experiment, the switch is pulsed on at sequentially delayed 50 ns increments beyond the time of ionization. The pulsing sequence is progressively increased to later and later times until all cations formed are directed away from the detector prior to the switch being turned on. The ionization laser

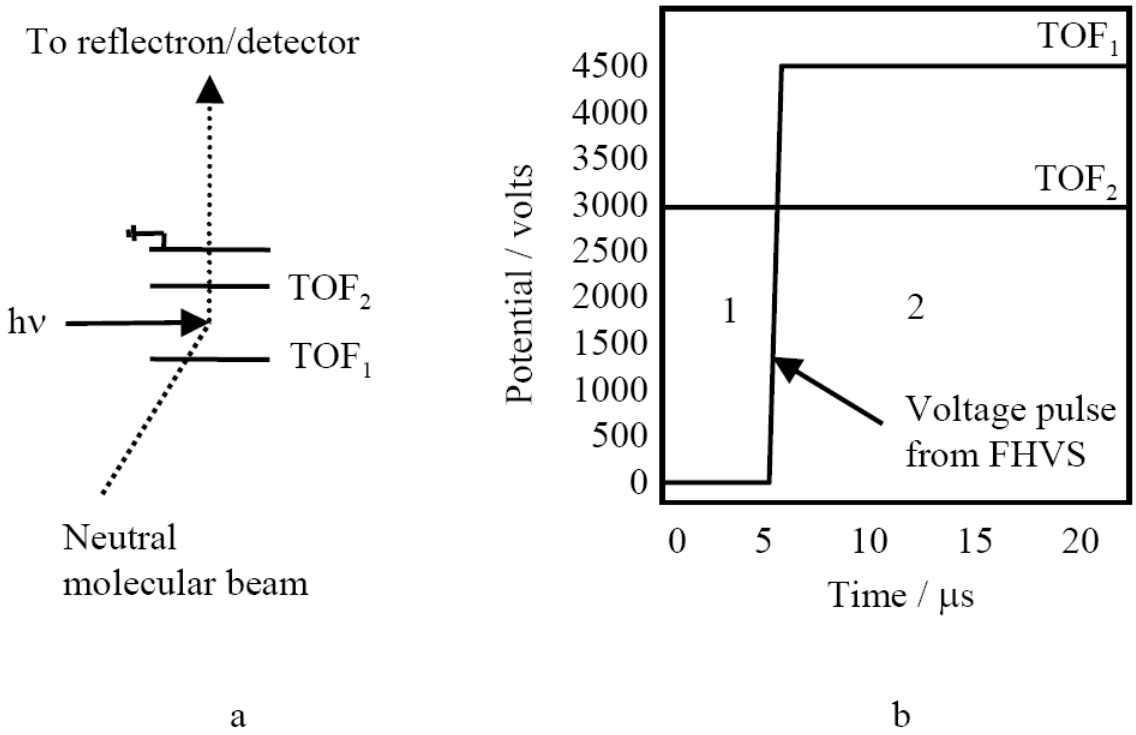

Figure **2.2**: a) A diagram of the ionization/acceleration region, where time-of-flight (TOF) grids accelerate ions either toward or away from the detector upon ionization of the neutral clusters. b) The potential on TOF 1 is pulsed by a fast high voltage switch (FHVS). This switch is stepped forward in time (50 ns steps) from a time prior to the ionization laser interacts with the molecular beam until ions are no longer detected. If the ionization laser interacts with the molecular beam in region 1, ions are directed away from the detector. The opposite is true for ions formed in region 2.

interacts with the molecular beam near TOF 1 in order to expedite the removal of ions. The manipulation of the potential on TOF 1 allows for the active study of delayed ionization.

2.3.2 Anion Mass Spectrometry

Modifications were made to the previously discussed experimental setup in order to perform anion mass spectrometry and as they will be discussed in this section. First, the reflectron was removed from the instrument. A microchannel plates detector connected to a metal anode (Del Mar Ventures, MCP-MA25) was installed at the top of the first time-of-flight region. During the anion spectrometry experiments, the first microchannel plate detector is kept at ground. The second plate is held at +1700 V and the electron collection plate is kept at +1800 V. In order to amplify the collected electrons while keeping a constant voltage on the collection plate, a special anion amplifier was built by the Research Instrumentation Facility at Penn State University. Anion mass spectrometry is required in order perform photoelectron spectroscopy on anion clusters, which is discussed in the next section.

Second, TOF 1 and 2 are equipped with a FHVS (Behlke, HTS-51) that allows for both grids to be held at ground potential to allow anions to enter the acceleration region. Then, TOF 1 and 2 are pulsed simultaneously to -1500 V and -1350 V, respectively. The voltage on TOF 2 and the timing of the pulse are adjusted to obtain the best resolution of the anion mass peaks in the mass spectrum. The electric field created by the potentials on

TOF 1 and 2 accelerate anions through the time-of-flight tube toward the microchannel plate detector.

2.4 Photoelectron Spectroscopy

The velocity map imaging (VMI) stack, displayed in Figure **2.3**, was installed at the end of the time-of-flight field-free region. At this point, the anions under study are separated by their mass. The VMI stack consists of three stainless steel plates, a time-of-flight tube, a position sensitive microchannel plates detector coupled to a phosphor screen and a CCD camera. The three plates extract the photodetached electron and accelerate it down a field-free flight tube toward the position sensitive microchannel plates detector. Upon collision with the detector, electron cascading occurs and the resulting electrons are directed to the phosphor screen. The phosphor screen emits photons in the position in which an electron collides into it. The CCD camera takes images of the photon output and sends the information to a computer to be analyzed.

The stainless steel plates are four inches in diameter and 0.04 inches thick. All three plates are isolated from one another and are separated by one-inch spacers made of Vespel^{TM}. The first plate is referred to as the repeller plate and is solid. The middle and last plate have a one inch hole in the center to allow for the passage of electrons. The last plate is referred to as the extraction plate, and it is physically and electronically connected to the time-of-flight tube. The repeller plate is held at ground potential prior to the anions entering the acceleration region between the repeller and the middle plate. Then, at the time of photodetachment, the plate is pulsed to ~-150 V by a fast high

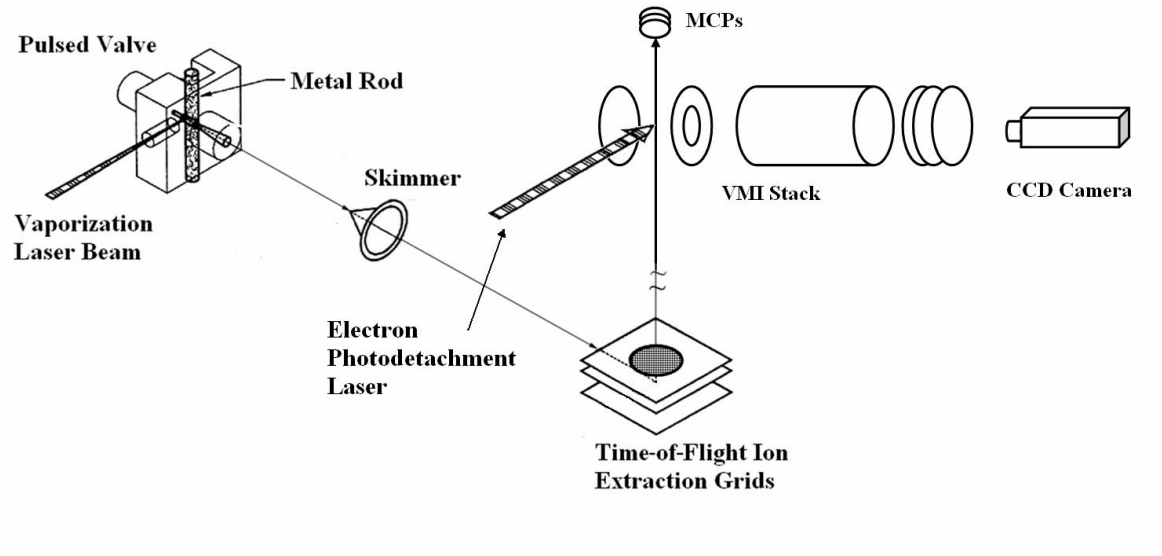

Figure **2.3**: Diagram of the instrument following addition of velocity map imaging (VMI) stack. A laser vaporization source is coupled to an anion time-of-flight mass spectrometer, which is equipped with a velocity map imaging apparatus.

voltage switch (Directed Energy, Inc., PVM-4210). The middle plate is held at ground potential, and the extraction plate and the time-of-flight tube is held at about ~400 V. The potentials are selected so that a photodetached electron with a given kinetic energy is accelerated to a point on the detector equidistant from the center of the detector as all other electrons emitted with the same excess kinetic energy irregardless of the electron's starting position.

Since the anions are separated in time by their mass, a packet of ions of a single mass are intersected at a 90^{o} angle by the second harmonic of a Nd:YAG laser (Specta Physics GCR-150). The polarization of the light is parallel to the plane of the phosphor screen. This laser is the same laser that was previously used to vaporize the metal rode in the laser vaporization source. In the photoelectron spectroscopy studies, a 10 Hz. Nd:YAG laser (Spectra Physics, DCR-2(30)) is used as the laser ablation laser in the cluster source.

The flight tube is three inches in diameter and five inches in length. Thin sheets of μ-metal reside inside and outside of the flight tube, which provide a shield from external magnetic fields. The three stainless steel plates are also surrounded by a μ-metal cup which is connected physically, yet electronically isolated, to the time-of-flight tube. This cup has two holes to allow for the passage of the anions under study as well as two other holes that allow for the intersection of the anions at a 90^{o} angle by the Nd:YAG laser.

The microchannel plates detector and phosphor screen were fabricated and mounted on a six inch conflat flange by Burhle Electro-Optics, Inc. (APD 3040FM). The flange contains a glass center so that the phosphor screen can be viewed from the outside

of the chamber. The front microchannel plate is held at a potential equal to that of the time-of-flight tube. The back microchannel plate is kept at a potential ~1600 V above that of the front microchannel plate and is pulsed up to ~1900 V above the front plate for ~200 ns (Directed Energy, Inc., PVM-4140) while the electrons under study impact the detectors. The potential difference between the front and back microchannel plate determines the quantity of electron gain that is provided by the detectors. Therefore, the increase in potential on the back microchannel plate allows for an increased gain in electronic signal when the electrons under study are impacting the detector, which allows for a decrease in background signal at all other times. The electrons that are emitted from the back microchannel plate are attracted to the phosphor screen (p47) that is held at ~-5200 V. At the position where the electrons impact the phosphor screen, photons are emitted from the back side of the screen. Importantly, this detector is position sensitive, and the photons are collected in images taken by a charge coupled device (CCD) camera (LaVision, Imager Intense). The CCD camera has a resolution of 1376 x 1040. The pixels are 6.45 μm x 6.45 μm. The CCD camera is setup to collect hundreds of images collected with a one second exposure time. The images are summed in order to sample thousands of laser shots.

2.5 References

1. J. R. Stairs and A. W. Castleman, Jr., Int. J. Mass. Spectrom. **216**, 75 (2002).

2. W. C. Wiley and I. H. McLaren, Rev. Sci. Instr. **26**, (12), 1150 (1955).

Chapter 3

The Origin of the Delayed Atomic Ion

3.1 Introduction

The ability of clusters to delay ionize (up to microseconds) was first observed in 1986 by Dao and Castleman in ionization studies of clusters comprised of paraxylene bound to trimethyl amine.[**1**] Dao and Castleman observed long tails to the slow side of trimethylamine ions which were attributed to its delayed ionization relaxation pathway. Shortly thereafter, Nieman *et al.*, examined this phenomenon in transition metal oxide clusters following multiphoton excitation.[**2**] Since then, many studies on metals,[**3**][**4**] fullerenes[**5**][**6**][**7**][**8**][**9**] and metal-carbon systems[**10**][**11**][**12**][**13**] have shown that these cluster systems also undergo an analogous relaxation mechanism. Generally, favorable candidates to display delayed ionization characteristics are clusters containing a significant number of vibrational modes. Furthermore, the magnitude of the cluster's ionization potential must be in competition with its binding energy, whereby dissociation is impeded compared to ionization. A substantial body of research has been focused on determining the mechanism of this delayed ionization phenomenon in clusters.[**14**] The mechanism most commonly used to explain the delayed emission of electrons is termed thermionic emission. Thermionic emission occurs when a hot system stores energy in its vibrational modes causing a delayed statistical ionization cooling mechanism. In order to account for the small, finite size of clusters; Klots[**15**] modified the conventional

Richardson-Dushman equation, which describes the thermionic emission of particles from a metallic surface when heated.

Ongoing experimentation in the Castleman group has focused on the delayed ionization properties of early transition metal-carbon clusters.[**10**][**11**][**12**][**16**][**17**] In systems that contain the Met-Car (M_8C_{12}, where M is Ti, Zr, or V) a delayed atomic ion is also observed, in addition to the delayed electron emission process.[**10**][**11**] Since this discovery, a considerable amount of scrutiny has been focused in an attempt to explain this delayed atomic ion. Hot atoms only cool via prompt ionization unless singlet-triplet effects are present, or rapid radiative emission occurs. Atoms do not contain any vibrational modes, which are required to thermionically emit electrons. Therefore, the delayed atomic ion must be a product of cluster that undergoes the delayed emission cation metal atoms.

There has been some evidence that the origin of the delayed atomic ion is related to the Met-Car. In one study, it was shown that the birth potentials of the delayed Met-Car and the delayed atomic ion were essentially identical.[**10**] Furthermore, studies have revealed when source conditions are such that the production of the Met-Car is favored, the delayed atomic ion is observed. Alternatively, if the source conditions are such that metal carbides of the form $(MC)_n$ are dominant species, the delayed atomic ion is not observed. However, in the aforementioned experiments, the Met-Car was not the only species excited in the molecular beam, and the results of the experiments could not definitively establish whether the Met-Car was the source of the delayed atomic ion. In fact, studies have shown that the Met-Car, $M_8C_{12}^+$, fragments into $M_7C_{12}^+$ and M, where the metal-carbon cluster retains the charge due to it having a lower ionization potential,

and the metal lost in the dissociation process is in the neutral state.[**18**][**19**][**20**] Large metal-carbon clusters, M_xC_y, generally have lower ionization potentials than their corresponding monomers,[**21**] so fragmentation of a large metal-carbon cluster ion would not be expected to result in observation of the monomer cation, but rather the fragmentation would result in the detection of the $M_{x-1}C_y^+$ fragmented ion.

In this chapter, I delve further into the origin of the delayed atomic ion by simultaneously studying the delayed ionization of zirconium and titanium carbides using species produced with a mixed metal alloy rod in a standard laser vaporization source coupled to a time-of-flight mass spectrometer.[**22**] These experiments have provided the ability to observe, for the first time, both the zirconium and titanium delayed atomic ions concurrently. Through an extensive investigation of clusters formed under these conditions, the origin of the delayed atomic ions is elucidated.

3.2 Experiment

The apparatus used in this work is described in detail in Chapter 2; therefore, only a brief description is given. A 1:1 titanium:zirconium metal alloy rod is ablated in a laser vaporization source by the second harmonic of a Nd:YAG laser (532 nm), while undergoing rotation and translation. Simultaneously, methane (~15% seeded in helium) is pulsed over the rod whereupon the produced clusters are supersonically expanded into a vacuum chamber. The clusters are skimmed prior to the molecular beam traveling between two time-of-flight grids. The ions formed in the source are directed off axis, while the neutrals are ionized using a XeCl excimer laser (308 nm). The ions travel

perpendicular to the molecular beam down a field-free region, where they enter a reflectron. The reflectron deflects the ions through another field-free region prior to detection using a microchannel plate detector. The signal from the micro channel plates is collected, amplified and sent to the data acquisition card (Gage 12100) where each mass spectrum is averaged 300 times.

Delayed ionization is studied by manipulating the time-of-flight grid furthest from the detector (TOF 1); see Figure **3.1**. Generally, a potential of 4500 V is applied to this grid, while a constant 3000 V potential is placed on the grid closer to the detector (TOF 2). The consequent electric field accelerates cations toward the reflectron. During delayed ionization experiments, the potential on TOF 1 is applied using a fast high voltage switch (FHVS), which has a ~15 ns rise time and remains on for 12.75 μs prior to slowly decaying back to ground ~80 μs later. The grid is kept at ground potential when the switch is off, producing an electric field that directs cations away from the detector. Initially, the switch is turned on prior to the ionization laser interacting with the molecular beam. During the delayed ionization experiment, the switch is pulsed on at sequentially delayed 50 ns increments beyond the time of ionization. The pulsing sequence is progressively increased to later and later times until all cations formed are directed away from the detector prior to the switch being turned on. The ionization laser interacts with the molecular beam near TOF 1 in order to expedite the removal of ions. The manipulation of the potential on TOF 1 allows for the active study of delayed ionization.

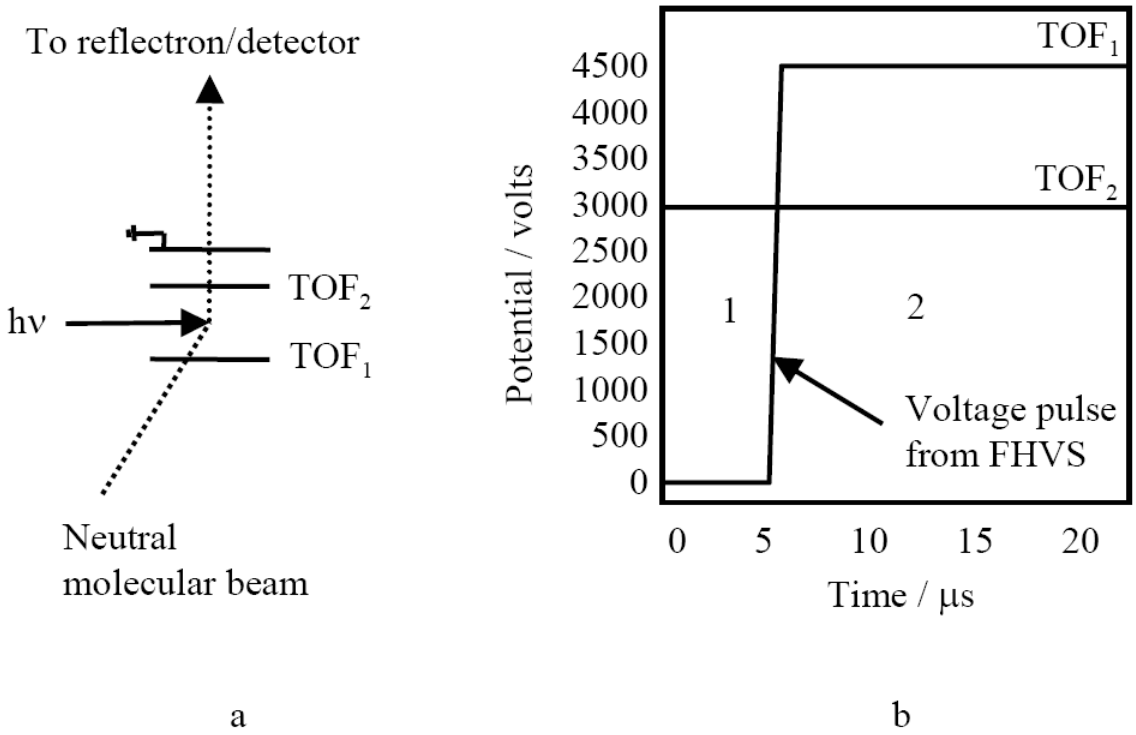

a b

Figure **3.1**: a) A diagram of the ionization/acceleration region, where time-of-flight (TOF) grids accelerate ions either toward or away from the detector upon ionization of the neutral clusters. b) The potential on TOF 1 is pulsed by a fast high voltage switch (FHVS). This switch is stepped forward in time (50 ns steps) from a time prior to the ionization laser interacts with the molecular beam until ions are no longer detected. If the ionization laser interacts with the molecular beam in region 1, ions are directed away from the detector. The opposite is true for ions formed in region 2.

3.3 Results and Discussion

Figure **3.2** displays the neutral clusters that are produced in the laser vaporization source and subsequently ionized. The mass spectrum shows the production of many zirconium-carbon clusters, including the zirconium Met-Car. However, regarding the titanium species, under the conditions of this experiment only the titanium monomer, titanium oxide and the titanium dicarbide are formed.

The three-dimensional plot in Figure **3.3** shows the mass spectra taken at each successive integral 50 ns time step of the FHVS. The mass spectra at early times are taken with the FHVS turned on before the ionization laser is imparted on the molecular beam, which allows the observation of all (both prompt and delayed) ions. When the prompt ions disappear from the mass spectrum, the FHVS is being turned on a sufficient time after the ionization laser interacts with the molecular beam to reject all of the prompt ions. Hence, any species that are observed in the mass spectrum at this point and thereafter are delay ionizing. The FHVS is turned on at later and later times until no species are being detected because all the ions formed by the ionization laser are being directed away from the detector.

In Figure **3.4** the natural logarithm vs. linear plots of the integrated delayed atomic ion intensities versus delay time for the aforementioned experiment are presented. Each point represents the sum of the species ionized at the time the switch is turned on and collected thereafter until the ion signal diminished to zero. Analysis of the data in Figure **3.3** must occur because the FHVS is on for microseconds, which causes the data in Figure **3.3** to represent the ions formed in a small window of time. First, the ion peak

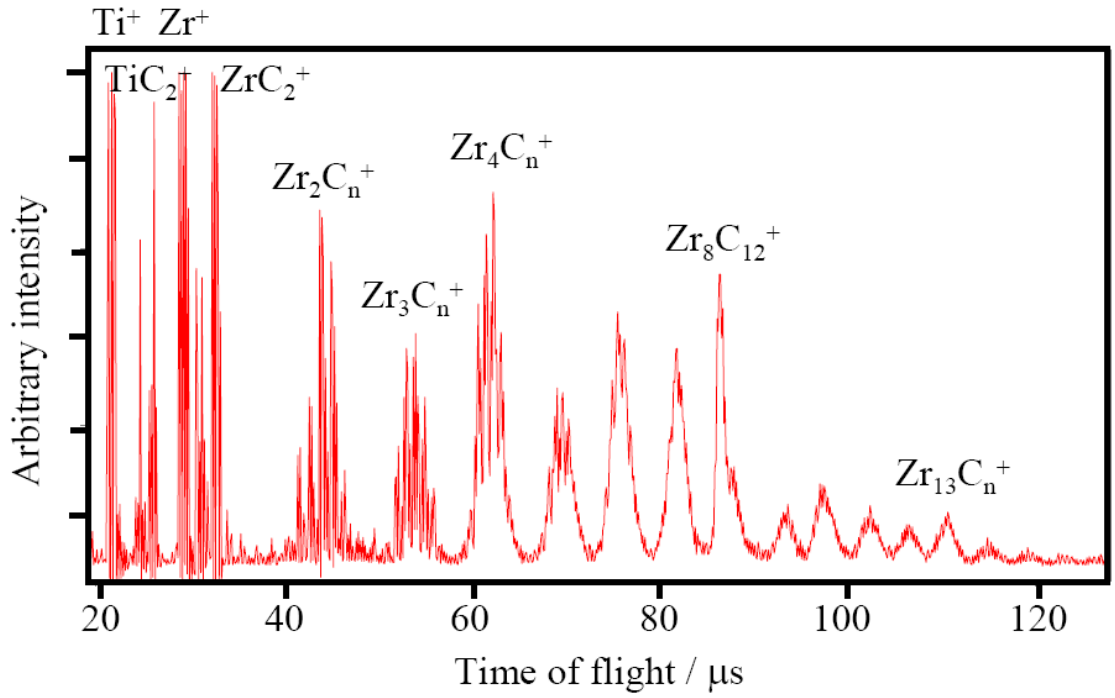

Figure **3.2**: Mass spectrum of titanium:zirconium mixed metal-carbon clusters using a 50:50 Zr:Ti mixed metal alloy rod in a laser vaporization source coupled to a time-of-flight mass spectrometer. The rod is vaporized by the 2nd harmonic (532 nm) of a Nd:YAG laser. The clusters are ionized by a XeCl excimer laser (308 nm).

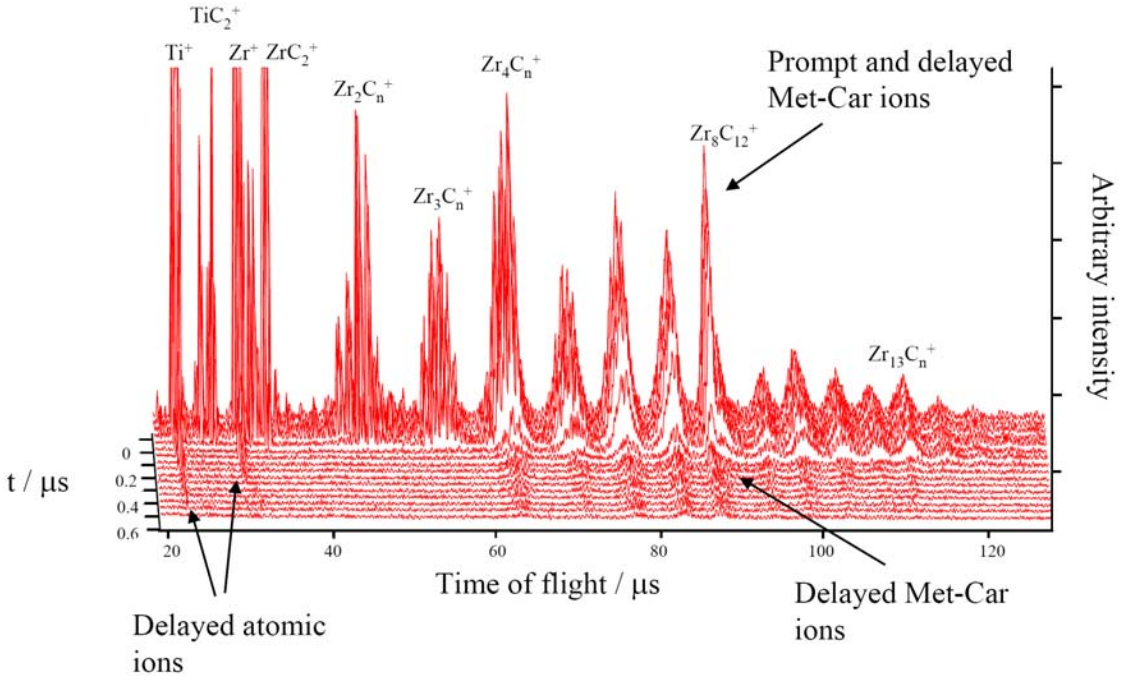

Figure **3.3**: Delayed ionization study of mixed metal-carbon clusters. Each mass spectrum represents the clusters that are in the acceleration region when the potential on the time-of-flight grid furthest from the detector (TOF 1) is pulsed to 4500 volts by a fast high voltage switch (FHVS) and therefore accelerated toward the detector. The electric field in the ionization region prior to the pulsing of the electric field is one that accelerates ions away from the detector. The timing (t) of the pulse from the FHVS is stepped forward in time in 50 ns steps until no further ions are detected. Time zero is the time at which the potential on TOF 1 is pulsed to 4500 volts and the ionization laser interacts with the molecular beam simultaneously. Spectra prior to time zero represent experiments wherein the potential on TOF 1 is pulsed to 4500 volts prior to the ionization laser interacting with the molecular beam.

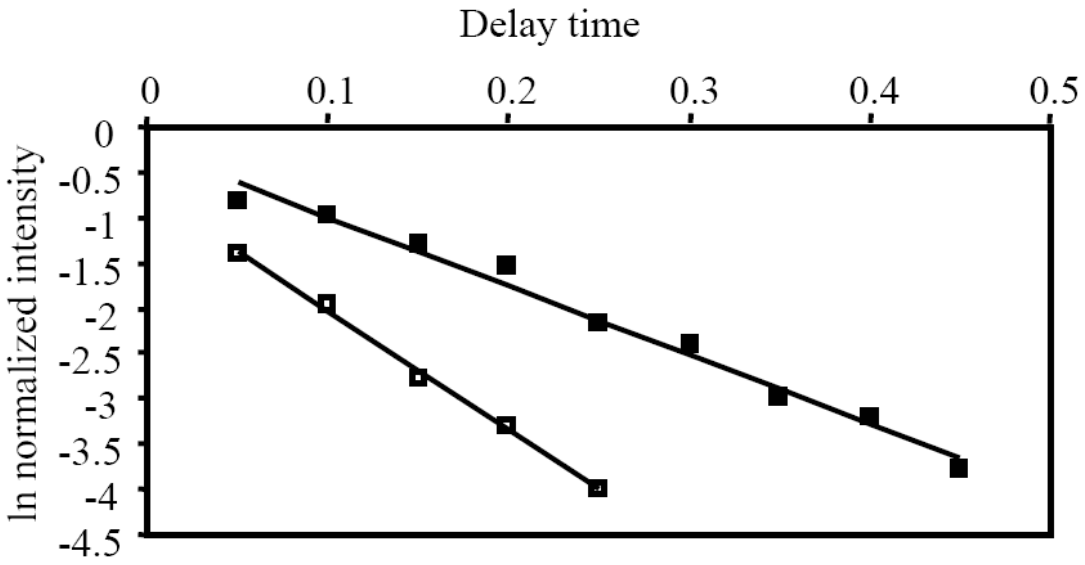

Figure **3.4**: Natural logarithm vs. linear plots of the integrated delayed atomic ion intensities vs. the timing in which the fast high voltage switch is turned on, accelerating ions toward the detector. Each point represents the ions formed at the time the switch is turned on and thereafter. Both the delayed atomic ions have linear relationships meaning that there is an exponential correlation between the intensity of the delayed atomic ions and the time at which they ionize. The filled squares represent the titanium delayed atomic ion and the open squares represent the zirconium delayed atomic ion. The lines are placed in the figure to guide the eye.

is integrated for each mass spectrum in Figure **3.3**. Second, the intensity at each time step is subtracted from the intensity at the previous time step. This allows for the determination of the intensity of the species ionized from one time step until the next time step (time-sliced intensities). Third, all the time-sliced intensities from each instant the FHVS is pulsed on until no more ions form, are summed together. Notice that both the delayed atomic ions have linear relationships meaning that there is an exponential correlation between the number of ions formed and the time at which they ionize, which is consistent with a first order statistical decay process.

Interestingly, no large titanium-carbon clusters are formed; however, both the zirconium and the titanium monomers are seen to delay ionize in Figure **3.3**. Therefore, the delayed titanium ion is likely a fragment of either the titanium oxide or the titanium dicarbide. The idea of the delayed atomic ion being the result of a dark cluster (one that never ionizes and therefore is not detected in the mass spectrum) is possible, but not probable due to the relatively large value of the ionization potential of the monomers when compared to larger metal-carbon clusters. One would expect a large metal-carbon cluster to ionize if it absorbs enough energy to ionize and fragment a metal monomer.

With the knowledge that the delayed titanium ion must originate from a light species, the ionization laser beam was refocused to interact with the front of the molecular beam where only the lighter species reside. Figure **3.5** shows the mass spectrum obtained at this region of the molecular beam. Notice the heavy mass clusters no longer interact with the ionization laser. Note that several oil peaks, which are observable and are inherent in the instrument; they do not contribute to delayed

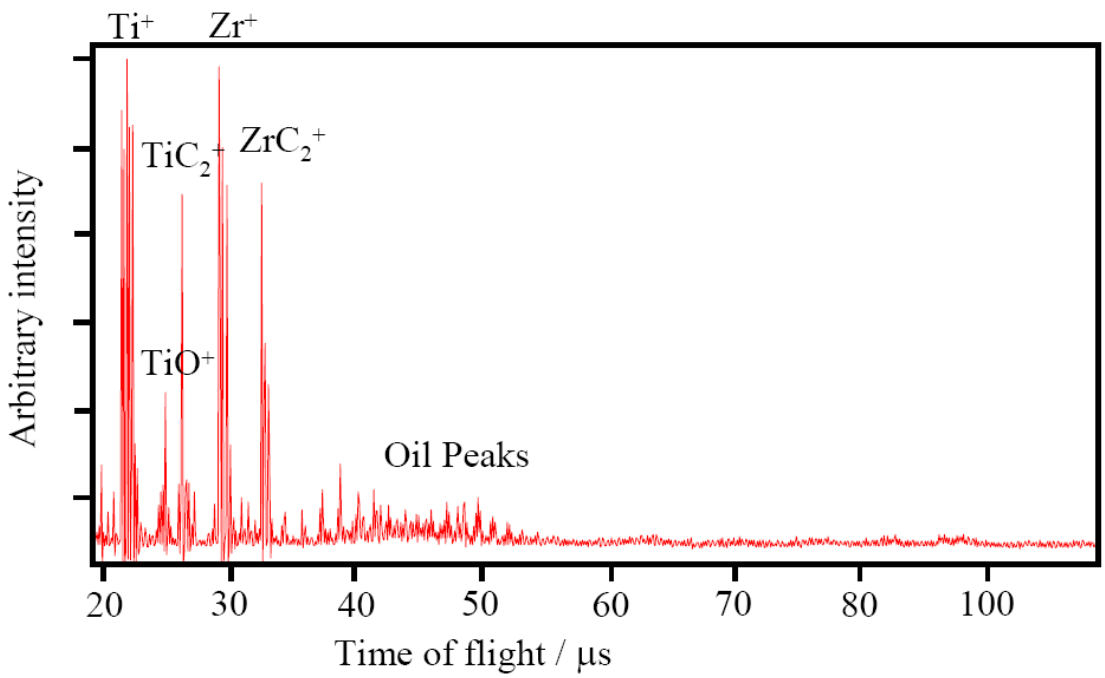

Figure **3.5**: Mass spectrum of titanium:zirconium mixed metal-carbon clusters using a 50:50 Zr:Ti mixed metal alloy rod in a laser vaporization source. The clusters are ionized by an excimer laser (308 nm), which was refocused in order to interact with only the low mass clusters. This laser position allows for the study of the delayed atomic ion without the excitation of larger species. Note that the several observable oil peaks, which are inherent in the mass spectrum, do not contribute to the formation of the delayed atomic ion.

ionization. Figure **3.6** displays the delayed ionization experiments accomplished with the ionization laser in the latter temporal position only exciting the light species in the molecular beam. No molecules larger than ZrC_2 are ionized; however, both delay atomic ions are still observed. The titanium and zirconium oxides form due to oxidation of the metal rod and were determined not to contribute to the delayed atomic ion following conclusive experiments whereupon helium was pulsed over the mixed metal rod and no delayed atomic ions were observed. Therefore, both delayed atomic ions are thought to be originating from an excited metal dicarbide complex. Moreover, this conclusion is consistent with the comparative intensities of the observed distributions.

There are three scenarios wherein a metal cation can be formed from a neutral metal dicarbide.

$$MC_2 \xrightarrow{h\nu} MC_2^* \xrightarrow{delay} M + C_2 \xrightarrow{fast} M^+ + C_2 \qquad \textbf{(3.1)}$$

$$MC_2 \xrightarrow{h\nu} MC_2^* \xrightarrow{delay} MC_2^+ \xrightarrow{fast} M^+ + C_2 \qquad \textbf{(3.2)}$$

$$MC_2 \xrightarrow{h\nu} MC_2^* \xrightarrow{delay} M^+ + C_2^- \qquad \textbf{(3.3)}$$

In all three scenarios, the metal dicarbide, MC_2, absorbs radiation and becomes an excited metal dicarbide, MC_2^*. Then, following a delay, three different scenarios are presented. Figure **3.7** displays an energy diagram of all three scenarios. The numbers in parentheses in Figure **3.7** are obtained via theoretical calculations. All other numbers are based on experimental data.

In Scenario **3.1**, the metal needs to gain enough energy to ionize following fragmentation. The delay occurs in the fragmentation step due to the high probability that the ionization of the metal ion is prompt. The fragmentation occurs long after the

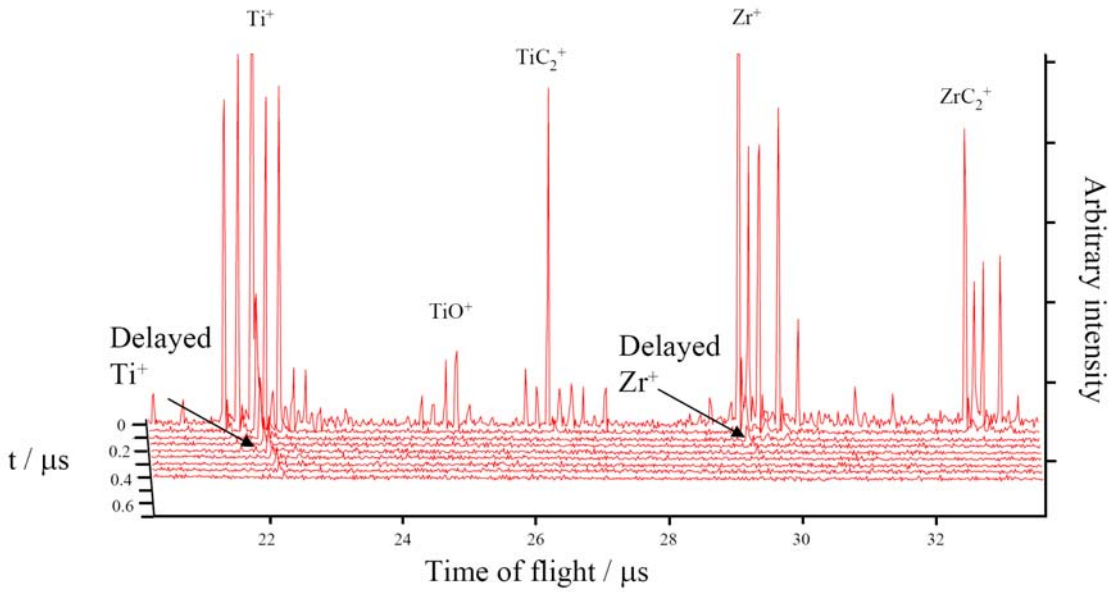

Figure **3.6**: Delayed ionization study of mixed metal-carbon clusters with the ionization laser refocused in order to interact with only the light species in the molecular beam. The delayed atomic titanium and zirconium ions are the only observable species in the mass spectrum that delay ionize. Both delay atomic ions are assumed to be brought forth through the same mechanism. Therefore, the only species that may contribute to the delayed atomic ions are of the form MC_2^+. The timing (t) of the pulse from the fast high voltage switch is stepped forward in time in 50 ns steps until no ions are detected.

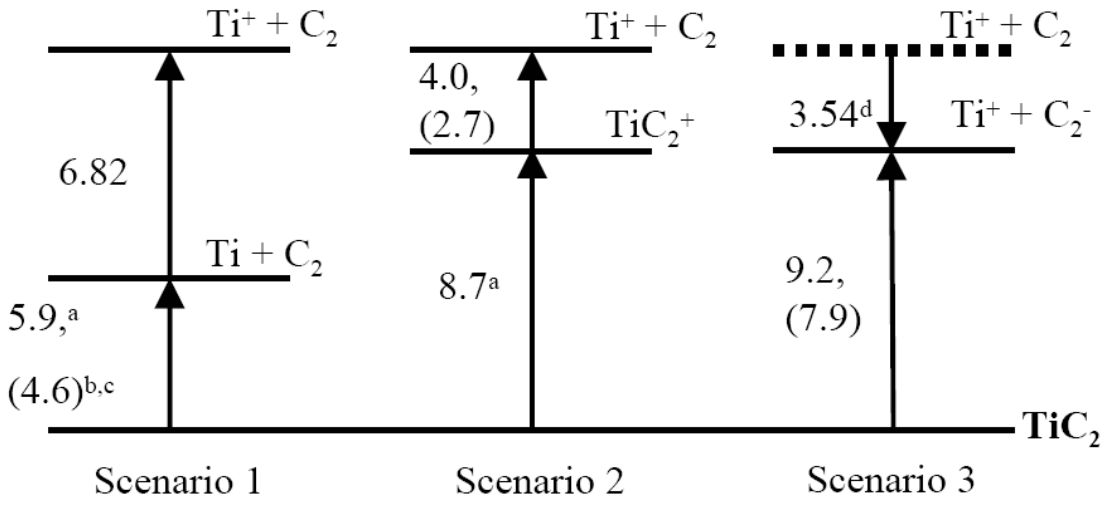

Figure **3.7**: Energy diagram portraying the three scenarios wherein a delayed titanium ion can be formed from a neutral titanium dicarbide. Note, all data are in eV, and the numbers in parentheses are based on theoretical calculations. All other numbers are based on experimental data. 1) Following a delay, the metal dicarbide fragments a titanium atom, which must fragment with sufficient energy to ionize. 2) The titanium dicarbide must store energy in its vibrational modes, although very few exist, for a significant period of time. Then, the titanium dicarbide delay ionizes and immediately fragments thereafter. 3) The titanium dicarbide is thought to be excited to a high Rydberg state just below its ionization potential, where it resides for a significant period of time. Next, the excited titanium dicarbide forms an excited ion-pair state and is subsequently separated into a carbon dimer anion and the delayed atomic cation. [a] refers to Ref. [**23**]. [b] refers to Ref. [**26**]. [c] refers to Ref. [**27**]. [d] refers to Ref. [**25**].

excitation laser has left the interaction region; therefore, the metal must fragment with enough energy to ionize, and ionize immediately, meaning the titanium dicarbide must initially absorb enough energy to complete both processes. Experiments have determined that the energy needed to dissociate a titanium atom from a TiC_2 molecule is 5.9 eV.[**23**] With the addition of the ionization potential of titanium (6.82 eV) to this fragmentation energy, Scenario **3.1** requires 12.7 eV of energy. The 4.0 eV energy difference between Scenario **3.1** and the direct ionization of the titanium dicarbide, which was experimentally determined to be 8.7 eV,[**23**] is quite large, and the two relaxation pathways are not thought to be in competition.

Scenario **3.2** involves the delay ionization of the titanium dicarbide, because any ion formed is immediately sent toward the detector. This eliminates the possibility of an ion delay fragmenting. Then, upon ionization, the TiC_2 unit must quickly fragment prior to the ion being accelerating toward the detector due to the electric field in the ionization region. The positive charge on the TiC_2 remains on the titanium due to the carbon dimer having an ionization potential of 12.15 eV.[**24**] Since, Scenario **3.2** starts with the identical reactants but takes a different route to equivalent products as Scenario **3.1**, Scenarios **3.1** and **3.2** can be estimated to require the same amount of energy to proceed from reactants to products even though they travel through a different intermediate state. Therefore, the energy required to fragment a titanium ion from a titanium dicarbide ion can be estimated to be 4.0 eV, which is determined by subtracting the ionization potential of TiC_2, 8.7 eV,[**23**] from the overall energy of Scenario **3.1**, 12.7 eV. Consequently, Scenario **3.2**, like Scenario **3.1**, is not an energetically favorable cooling mechanism due to it requiring 4 eV of energy more than the direct ionization of the titanium dicarbide. In

addition, if Scenario **3.2** were the proper mechanism for the origin of the delayed atomic ion, one would expect to see some delayed metal dicarbide prior to the fragmentation of a metal cation, which is not observed in the experiments. Furthermore, TiC_2 is not thought to have the number of vibrational modes necessary to thermionically emit electrons. Also, the idea of a metal atom delay ionizing due to a long lived triplet state is thought to be improbable.

In Scenario **3.3**, note that the carbon dimer is negatively charged. Since the carbon dimer has an electron affinity of 3.54 eV,[**25**] Scenario **3.3** requires only 9.2 eV of energy, which is only slightly higher than the experimental ionization potentials of titanium dicarbide. Therefore, Scenario **3.3** requires far less energy than Scenarios 1 and 2 due to the C_2 receiving an electron and the energy to ionize the metal monomer is no longer needed. A proposed reaction mechanism for Scenario **3.3** involves the absorption of enough energy by the titanium dicarbide to become excited into a high Rydberg state just below its ionization potential. Then, following a delay, the titanium dicarbide forms an energetic ion-pair that has enough kinetic energy to overcome the columbic attraction between the oppositely charged particles. This allows for the detection of a delayed titanium cation.

The experimentally determined energy needed to fragment a titanium atom from a titanium dicarbide is 1.3 eV higher than the theoretical fragmentation energy of 4.6 eV, which is obtained from the subtraction of the theoretical binding energy of C_2 (6.26 eV)[**26**] from the theoretical atomization energy of TiC_2 (10.9 eV).[**27**] Consequently, the theoretical energy needed to complete each scenario is lowered by 1.3 eV.

Titanium dicarbide is used in the three scenarios as an example due to the extensive amount of knowledge regarding this molecule. It is thought that the same scenario is responsible for the origin of the delayed zirconium and vanadium atomic ions as well.

3.4 Conclusions

The finding that the metal dicarbide is responsible for the delayed atomic ion explains the previous experiments wherein the delayed atomic ions were thought to be a fragment of the Met-Car, because the formation of the metal dicarbide is known to correspond with the formation of the Met-Car but not in source conditions that favor $(MC)_n$ clusters. Furthermore, the experimental findings presented herein are evidence toward the delayed atomic ion being formed through the energetically favorable Scenario **3.3** where the titanium dicarbide is excited into a high Rydberg state just below the TiC_2 ion state. Then, following a delay, an excited ion-pair complex is formed with enough energy to overcome the columbic attraction of the charged particles causing it to separate into a titanium cation and the carbon dimer anion. Scenarios 1 and 2, which involve both ionization and fragmentation, require the absorption of far greater energy than is required to remove an electron from a titanium dicarbide. Furthermore, the excited ion-pair state is facilitated by the extremely high electron affinity of the carbon dimer, 3.54 eV.[**25**] The search for other systems that may undergo a similar unique dissociation mechanism, wherein a delayed metal ion is emitted, is underway.

3.5 References

1. D. Dao and A. W. Castleman, Jr, J. Chem. Phys. **84,** 1435 (1986).

2. G. C. Nieman, E. K. Parks, S. C. Richtsmeier, K. Liu, L. G. Pobo, and S. R. Riley, High Temp. Sci. **22,** 115 (1986).

3. T. Leisner, K. Athanassenas, O. Echt, D. Kreisle, and E. Recknagel, J. Chem. Phys. **99,** 9670 (1993).

4. A. Amrein, R. Simpson, and P. Hackett, J. Chem. Phys. **95,** 1781 (1991).

5. E. E. B. Campbell, G. Ulmer, and I. V. Hertel, Phys. Rev. Lett. **67,** 1986 (1991).

6. D. Ding, J. Huang, R. N. Compton, C. E. Klots, and R. E. Haufler, Phys. Rev. Lett. **73,** 1084 (1994).

7. H. Lin, K.-L. Han, Y. Bao, E. B. Gallogly, and W. M. Jackson, J. Phys. Chem. **98,** 12495 (1994).

8. J. U. Andersen, P. Hvelplund, S. B. Nielsen, U. V. Pedersen, and S. Tomita, Phys. Rev. A **65,** 053202 (2002).

9. A. Lassesson, K. Mehlig, A. Gromov, H. Shinohara, and E. E. B. Campbell, J. Chem. Phys. **117,** 9811-9817 (2002).

10. B. D. May, S. F. Cartier, and A. W. Castleman, Jr., Chem. Phys. Lett. **242,** 265 (1995).

11. S. F. Cartier, B. D. May, and A. W. Castleman, Jr., J. Chem. Phys. **104,** 3423 (1996).

12. J. R. Stairs, K. M. Davis, S. J. Peppernick, and A. W. Castleman, Jr., J. Chem. Phys. **119,** 7857 (2003).

13. J. R. Stairs, S. J. Peppernick, K. M. Davis, and A. W. Castleman, Jr., Israel J. Chem. **44,** 223-228 (2004).

14. E. E. B. Campbell and R. D. Levine, Annu. Rev. Phys. Chem. **51,** 65 (2000). and references within.

15. C. E. Klots, Chem. Phys. Lett. **186,** 73 (1991).

16. S. E. Kooi and A. W. Castleman, Jr., J. Chem. Phys. **108,** 8864 (1998).

17. B. D. Leskiw and A. W. Castleman, Jr., C. R. Physique **3,** 251-272 (2002).

18. J. R. Stairs, K. M. Davis, and A. W. Castleman, Jr., J. Chem. Phys. **117,** 4371 (2002).

19. J. Purnell, S. Wei, and A. W. Castleman, Jr., Chem. Phys. Lett. **229,** 105-110 (1994).

20. S. Wei, B. C. Guo, J. Purnell, S. A. Buzza, and A. W. Castleman, Jr., J. Phys. Chem. **97,** 9559-9561 (1993).

21. In collaboration with Professor Jorge Sofo, unpublished calculations have shown the Ti_7C_{12}, which is the corresponding fragment of the Met-Car following fragmentation of a titanium monomer, has a significantly lower ionization potential than the titanium monomer.

22. K. M. Davis, S. J. Peppernick and A. W. Castleman, Jr., J. Chem. Phys. **124,** 164304 (2006).

23. C. A. Stearns and F. J. Kohl, High Temp. Sci. **2,** 274 (1970); **6,** 284 (1974).

24. V. H. Dibeler and S. K. Liston, J. Chem. Phys. **47,** 4548 (1967).

25. K. P. Huber and G. Herzberg, *Constants of Diatomic Molecules* (VanNostrand Reinhold Company, New York, 1979), p. 116 taken from Feldman, Zeitschrift Für Physik **25a,** 621 (1970).

26. E. G. Noya, R. C. Longo, and L. J. Gallego, J. Chem. Phys. **119**, 11130 (2003).

27. R. Sumath and M. Hendrickx, Chem. Phys. Lett. **287,** 496 (1998).

Chapter 4

Evidence of Ion-pair Separation in Photoexcited Metal-Carbon Clusters

4.1 Introduction

Two major relaxation pathways that a molecule may undergo upon photoexcitation in the gas phase are ionization and neutral fragmentation. Photoionization of clusters and molecules is a popular research field and provides the means for detection of the clusters under study in the previous chapters of this thesis. Neutral fragmentation, on the other hand, is a much more difficult relaxation pathway to study. In a molecular beam time-of-flight mass spectrometry experiment, a cluster that is photoexcited and subsequently fragments into smaller neutral units remains undetected and goes unnoticed. Two minor relaxation pathways that are often disregarded in cluster research are radiative emission and ion-pair separation. Ion-pair separation, which involves the production of both a cation fragment and an anionic fragment following excitation, may also occur. The mechanism is often disregarded due to it having little significance in the production of cations compared to prompt ionization. However, in special cases where a molecule is excited to or around its ionization potential and there is a highly electronegative species present, ion-pairs are formed and negative ions have been detected.

In an experiment studying photoionization efficiency curves of thallium iodide using a vacuum-ultraviolet monochromator coupled to a mass spectrometer and a

molecular-beam source, Berkowitz and Chupka found an ion-pair state at 5.79 eV producing a Tl^+ and a I^- atoms as its products.[**1**]

In another experiment in search of photoionization efficiency curves of OClO, Rockland and coworkers report both O^- and Cl^- fragments following photoexcitation at different wavelengths. The detection of negative ions following neutral photoexcitation is evidence of ion-pair separation.[**2**]

Theoretical calculations performed by Levine and co-workers suggest that ion-pair separation should be considered as an important relaxation mechanism of molecules when photoexcitation occurs above the ionization potential of the molecule understudy, particularly, when the molecule's ion-pair formation energy is comparable to its ionization potential. The computational examples that were studied to reach this conclusion were O_3, Cs_2, and HNO_2.[**3**]

In the previous chapter, the delayed atomic ion was proposed to be the product of a delayed ion-pair separation that is formed due to the excitation of the MC_2 molecule to a compilation of Rydberg states near the ionization threshold. In this chapter, the detection of C_2^- following excitation of M_xC_y clusters provides further evidence of this mechanism being the source of delayed M^+ that has been detected in previous photoexcitation studies of metal carbides.

4.2 Experiment

The apparatus used in these experiments is a standard time-of-flight (TOF) mass spectrometer coupled to a laser vaporization source. Within the source, a 1:1

titanium:zirconium metal alloy rod is ablated by the second harmonic of a Nd:YAG laser (532 nm), while rotating and translating in order to ensure a new spot on the rod is ablated in each experiment. Simultaneously, methane (~15% seeded in helium) is pulsed over the rod. The clusters are formed in a region near the rod prior to supersonically expanding into a vacuum chamber. The ions formed in the source are directed off axis by a deflection rod. The neutral clusters are skimmed creating a molecular beam, which travels between two TOF grids, whereupon they are excited using a XeCl excimer laser (308 nm).

Cations are given a birth potential of approximately +3750 V in order to accelerate the ions perpendicular to the molecular beam down a field-free region, at the point they are detected using a micro channel plate (MCP) detector. In order to detect anions, the potential on the TOF grids are switched to a negative potential, giving ions formed a -3750 V birth potential, which causes cations to be directed away from the detector and anions toward the detector. The first MCP plate is held at a potential of -1750 V, the second MCP plate is given a potential of -100 V, and the collection plate is grounded. This is a common setup used to detect cations; however, due to the high birth potential of the ions in these experiments, anions are able to be detected as well. The signal from the micro channel plates is collected, amplified and sent to the data acquisition card (Gage 12100) where each mass spectrum is averaged 300 times.

4.3 Results and Discussion

A major relaxation mechanism that occurs when neutral clusters are photoexcited is ionization, whereupon a neutral cluster ejects an electron and becomes a cation. Generally, this mechanism, along with neutral fragmentation, is the primary mechanism for a molecule or cluster to relax upon excitation. Figure **4.1** is a time-of-flight mass spectrum of cations formed upon excitation of a neutral molecular beam of mixed metal-carbon clusters by a XeCl excimer laser (308 nm), which demonstrates the first major relaxation pathway. Furthermore, a cluster has the ability to form an ion-pair and separate. Ion-pair separation occurs when an ion-pair excited state lies at or near the cluster's ionization potential. Figure **4.2** is a time-of-flight mass spectrum of anions detected under the same experimental conditions as above excluding the extraction region, where the TOF grids have negative potentials in order to give anions a negative birth potential to direct anions toward the detector rather than cations. This mass spectrum represents ions formed via ion-pair separation.

The detection of the carbon dimer anion supports the hypothesis presented in the last chapter, where a delayed atomic cation was thought to arrise due to the separation of a metal dicarbide into a metal cation and a carbon dimer anion. The detection of the larger carbon cluster anions was unexpected. This discovery reiterates the idea of ion-pair separation being a competing relaxation mechanism when photoexcitation of a neutral cluster occurs. The source of these larger carbon anion fragments would be an interesting avenue of research if one had the ability to mass select anion clusters prior to excitation, which is beyond the abilities of the current experiment setup.

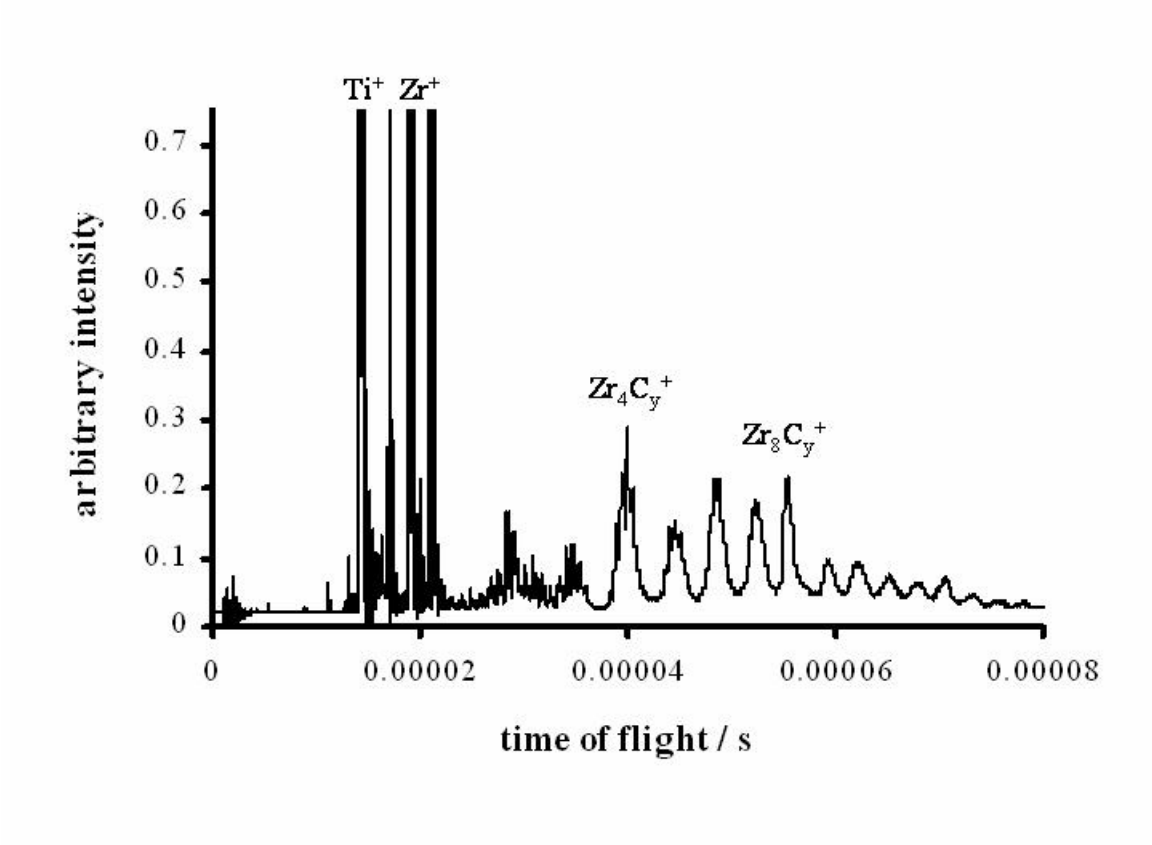

Figure **4.1**: Time-of-flight mass spectrum of cations detected following excitation of a neutral molecular beam of $Ti_xZr_yC_z$ clusters with a XeCl excimer laser (308 nm).

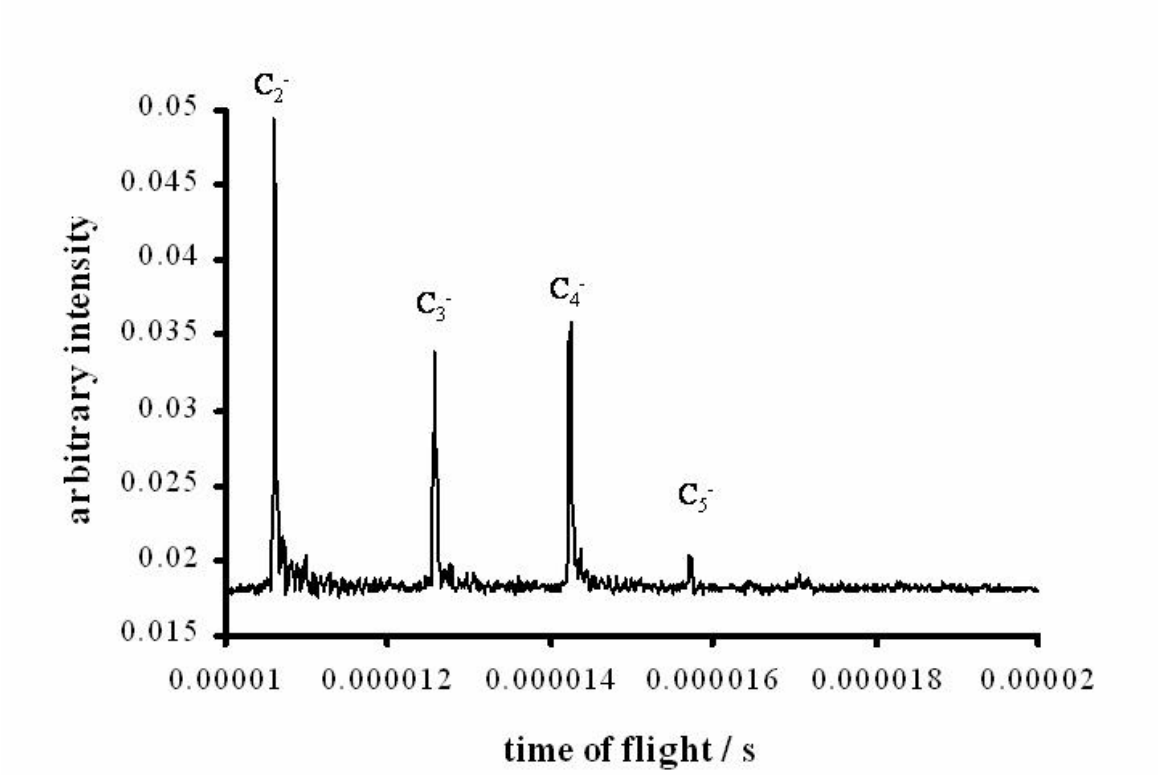

Figure **4.2**: Time-of-flight mass spectrum of anions detected following excitation of a neutral molecular beam of $Ti_xZr_yC_z$ clusters with a XeCl excimer laser (308 nm).

4.4 References

1. J. Berkowitz and W. A. Chupka, J. Chem. Phys. **45**, 1287 (1966).

2. U. Rockland, H. Baumgärtel, E. Rühl, O. Lösking, H S. P. Müller and H. Willner, Phys. Chem. Chem. Phys. **99**, 969 (1995).

3. N. Ohmichi, J. Silberstein, and R. D. Levine, J. Phys. Chem. **85**, 3369 (1982).

Chapter 5

Design of the Velocity Map Imaging Apparatus

5.1 Introduction

The purpose of this chapter is to give details concerning the instrumental design of a velocity map imaging apparatus, which performs photoelectron spectroscopy on anion atoms and ultimately clusters. The velocity map imaging stack is displayed in detail in Figure **4.1**. A molecular beam of the anion under study, R^-, enters the extraction region perpendicular to the flight tube. In the center of the extraction region, an electron is removed from the R^- anion under study via laser induced photoexcitation. A two stage electric field extraction region accelerates the electron through a field-free time-of-flight tube toward a position sensitive microchannel plate (MCP) detector coupled to a phosphor screen. A charge coupled device (CCD) camera is setup outside of the vacuum chamber and collects images of the extracted electrons. The output is an image that contains information regarding the cluster's photoelectron spectrum. In order to extract information from the image, a general understanding of the experiment is needed. Each detached electron has a kinetic energy (KE) given by

$$KE = nh\nu - BE - E_{int} \qquad (\mathbf{5.1})$$

where $nh\nu$ is the number of photons absorbed, BE is the binding energy of the electron and E_{int} is the internal energy of the neutral product. The electric fields in the extraction

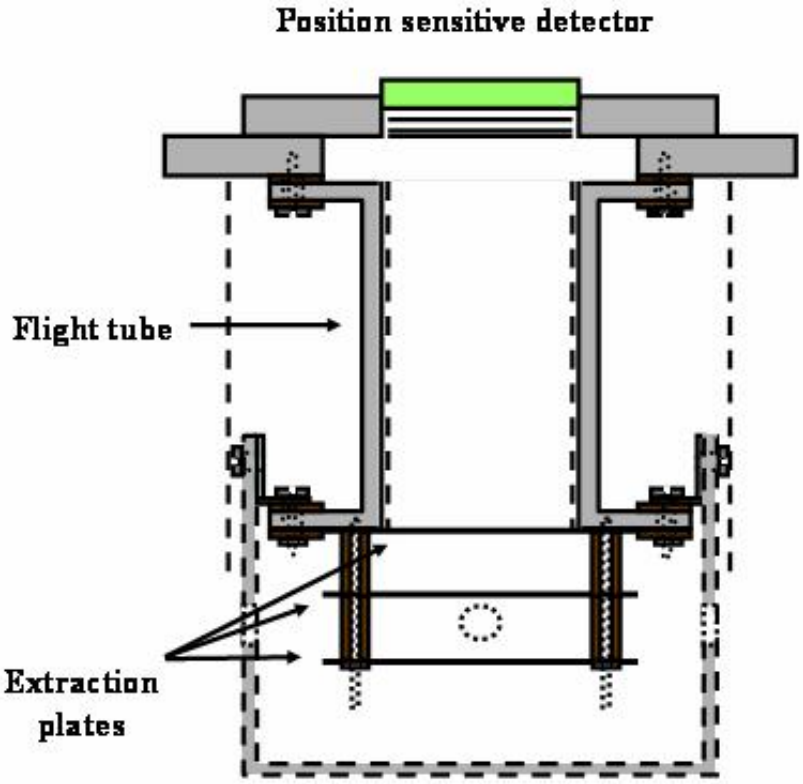

Figure **5.1**: Cross-section of the velocity map imaging apparatus. The dashed lines represent magnetic shielding.

region map an electron with a particular kinetic energy to a specific point on the position sensitive detector. As the photodetached electrons travel down the flight tube, they act as an expanding Newton sphere (see Figure **4.2**). Electrons having different kinetic energies expand at different rates; therefore, the photodetached electrons with different kinetic energies contact the detector at a different distance from the center of the detector. The result is a 2-D image that is a projection of the 3-D Newton spheres of electrons. Using the inverse Abel transform, the 3-D Newton spheres are reconstructed, and a slice from the center of the 3-D Newton sphere results in a "reconstructed image". The reconstructed image provides angular and kinetic energy information of the photodetached electrons.[**1**]

Calibration of the instrument requires photodetachment of electrons from an atomic anion with known electron binding energies. In studies conducted on the velocity map imaging instrument, copper was used for calibration. The copper anion has an electronic configuration of $3d^{10}4s^2\ ^1S_o$ and has an electron affinity of 1.236 eV, which represents the transition from the anion ground state to the neutral ground state that has an electron configuration of $3d^{10}4s^1\ ^2S_{1/2}$.[**2**]

5.2 Experimental Design

The extraction region of the velocity map imaging stack (see Figure **4.1**) consists of two different electric fields that accelerate the photodetached electron down a field-free time-of-flight tube. Potential is applied to three stainless steel electrodes to create these electric fields. The first extraction region is the region in which the electron is removed

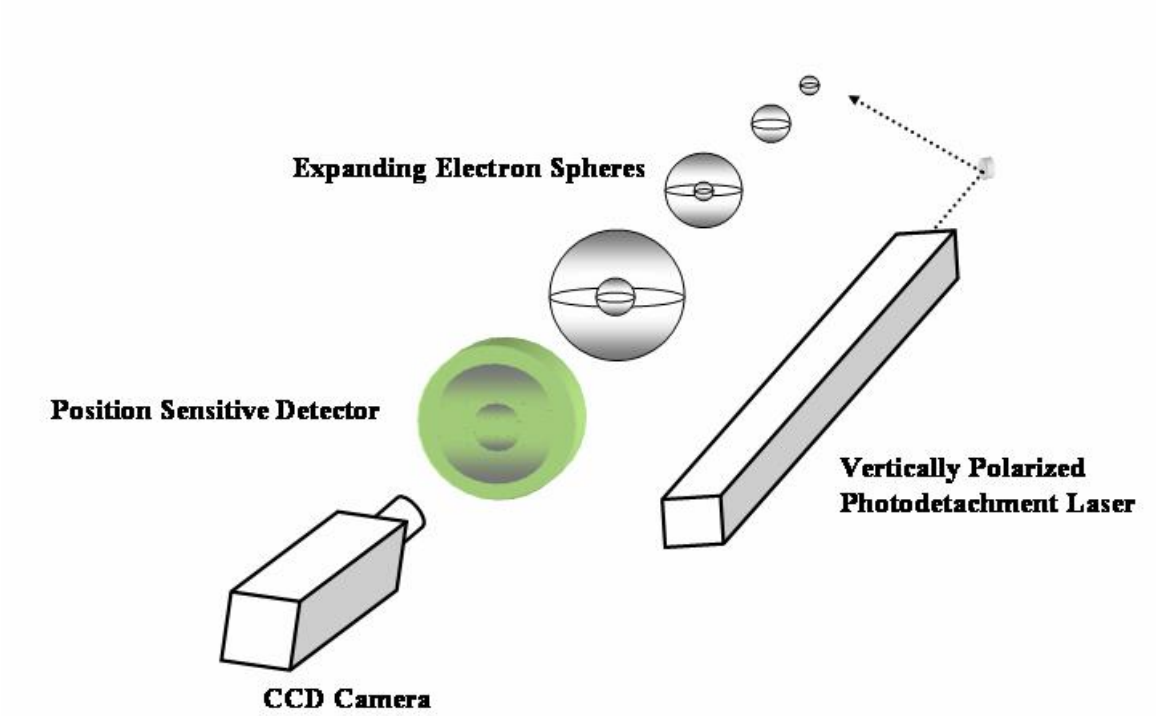

Figure **5.2**: Diagram portraying the expanding electron spheres that contain information regarding the kinetic energy of the photodetached electron as they travel toward a position sensitive detector in the velocity map imaging apparatus. The larger sphere represents electrons with a given kinetic energy higher than those contained within the smaller sphere.

from the anion. The repeller plate is the stainless steel electrode furthest from the detector and has a negative potential applied to it in order to repel electrons toward the detector. The middle plate is held at ground potential. The third electrode is the extraction plate and it is held at a positive potential to attract electrons toward the detector. All three plates are four inches in diameter and 0.04 +/- 0.005 in. thick. The repeller plate is solid stainless steel, while the middle plate and the extraction plate have a one inch in diameter hole in their center to allow for the passage of electrons. Both sides of each electrode have been polished (AB Precision) to ensure complete flatness and accurate thickness. Each plate has four 1/8 in. in diameter clearance holes located 1/8 in. from the edge of the plate separated from each other by 90^{o}. An 0-80 molybdenum threaded rod (Thermo Shield) connects the three plates to the time-of-flight tube. The extraction plate is electronically and physically attached to the flight tube. The middle plate is separated from the extraction plate and the repeller plate by a 1 +/- 0.02 in. Vespel^{TM} spacer (McMaster-Carr). Vespel^{TM} is a machinable insulator that acts to electronically isolate the middle plate and the repeller plate. A ceramic rod surrounds the 0-80 molybdenum threaded rod to ensure that each plate does not contact the 0-80 threaded rod and remains isolated. An 0-80 molybdenum nut (Thermo Shield) holds the three plates and spacers against the time-of-flight tube. A Vespel^{TM} spacer separates the washer from the repeller plate.

The field-free time-of-flight tube is a stainless steel cylinder that is three inches in diameter and five inches in length. The flight tube is held at the same positive potential as the extraction plate and the front plate of the microchannel plate detector which acts as the beginning and end of the field-free region, respectively. Attached to the flight tube is

a μ-metal cup (Amuneal), which is isolated from the flight tube and is held at ground potential. The cup surrounds the three extraction plates and shields the region from magnetic fields that alter the path of electrons. There are four holes in the μ-metal cup located 90^{o} from each other to allow for the passage of the photodetachment laser and the anions perpendicular to one another. Four sheets of μ-metal (Amuneal, each sheet has a dimension of 30 in. x 14 in. x 0.02 in.) also shield the flight tube and microchannel plate detectors from stray magnetic fields. Two μ-metal sheets are located inside the flight tube, while two more sheets are fastened to the outside of the μ-metal cup and extend to the eight inch reducing flange. The flight tube is attached to an eight inch reducing flange using 4-40 titanium screws (United Titanium). The flight tube is isolated from the flange using a ceramic spacer surrounding the screw as well as two Vespel^{TM} washers.

The Chevron^{TM} Model 3040FM detector assembly (Burle Industries, Inc.) contains two position sensitive microchannel plates coupled to a P47 phosphor screen mounted to a six inch conflat (CF) flange. A glass window in the center of the six inch flange, next to the phosphor screen, allows images to be viewed from outside the vacuum chamber. The high voltage feedthroughs are mounted to the edge of the flange. This setup is purchased preassembled; therefore, no machining modifications to the six inch flange are possible.

A CCD camera (Imager Intense, LaVision) is used to acquire images displayed on the phosphor screen. The CCD camera has a resolution of 1376 x 1040 with each pixel having a size of 6.45 μm x 6.45 μm. A focusing lens (Schneider, Xenon CM 120 10456 F0.95 17mm, order # 21-010456) is attached to the CCD camera. DaVis software

(LaVision) is a 32bit software for image acquisition and processing. The software also controls the hardware components on the camera.

The velocity map imaging stack is contained within a customized 6-way cross (Nor-Cal Products) as seen in Figure **5.3**. The 6-way cross contains three 2 ¾ in. CF flanges, two six inch CF flanges and one eight inch CF flange. Attached to two of the 2 ¾ in. flanges are a CF to quick-connect coupling adaptor (Kurt J. Lesker, F0275xvc100), which allows for the installation of a one inch in diameter stainless steel tube containing a quartz slide (ChemGlass, CGQ-0640-02). The quartz slides act as laser ports to allow the photodetachment laser to enter and exit the chamber. The third 2 ¾ inch flange has a flange that contains four MHV high voltage feedthroughs attached to it. The MHV feedthroughs are electronically connected to the three extraction plates in the velocity map imaging stack to allow for a potential to be applied to them. One of the six inch flanges is attached to the anion time-of-flight tube. The other six inch flange is attached to a blank six inch flange that has a microchannel plate detector (Del-Mar Ventures, MCP-MA 24/2) attached to it to allow for the detection of anions passing through the imaging stack. The eight inch flange is connected to the eight inch reducing flange that contains the velocity map imaging stack. Figure **5.4** is a diagram of the instrument following the installation of the velocity map imaging.

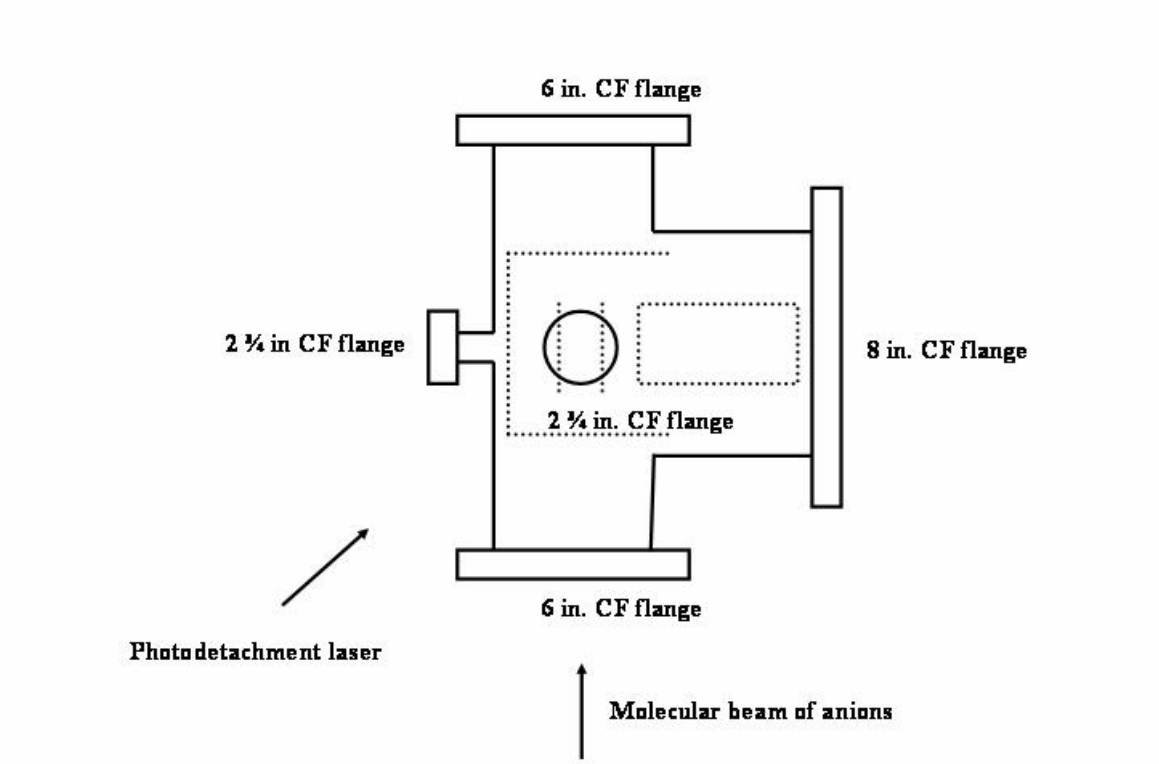

Figure **5.3**: Custom chamber that contains the velocity map imaging stack. The photodetachment laser enters the chamber perpendicular to the page through the two 2 ¾ in. Conflat (CF) flanges (the exit 2 ¾ in. is not shown in this diagram).

5.3 Operation and Calibration

Copper anions are formed via the method described in Chapter 2. A rotating and translating copper rod is ablated with the second harmonic (532 nm, 50 mj/pulse) of a pulsed Nd:YAG laser (Spectra-Physics, DCR-2(30)). Producing copper anions does not require gas to be pulsed over the rod. Copper anions are accelerated down a field-free flight tube by a two-stage acceleration region where they enter the velocity map imaging stack. The copper anions are photoexcited by the second harmonic (532 nm, 50 mj/pulse) of a pulsed Nd:YAG laser (Spectra-Physics, GCR-150). At the time in which the electrons are removed from the copper anions, the repeller plate is pulsed from ground potential to approximately -150 V via a fast high voltage switch (FHVS, Directed Energy, PVM-4210). The middle plate is held at ground potential, while the extraction plate, time-of-flight tube and front MCP plate are given a potential of 400 V. The photodetached electrons are accelerated toward the position sensitive MCP detector coupled to a phosphor screen and images are collected using a CCD camera. The back MCP plate is pulsed from 1600 V to 1900 V for ~200 ns (Directed Energy, Inc., PVM-4140) while the photodetached electrons arrive, and then it is pulsed back to 1600 V. This voltage setup limits the amplification of background electrons.

Figure **5.5** displays a raw image of the photodetached electrons of Cu^- under the previously described experimental conditions. Figure **5.6** is the reconstructed image using BASEX software.[**3**] BASEX software uses a Gaussian basis-set expansion to reconstruct Abel-transformable images. The raw image represents a 2-D projection of a

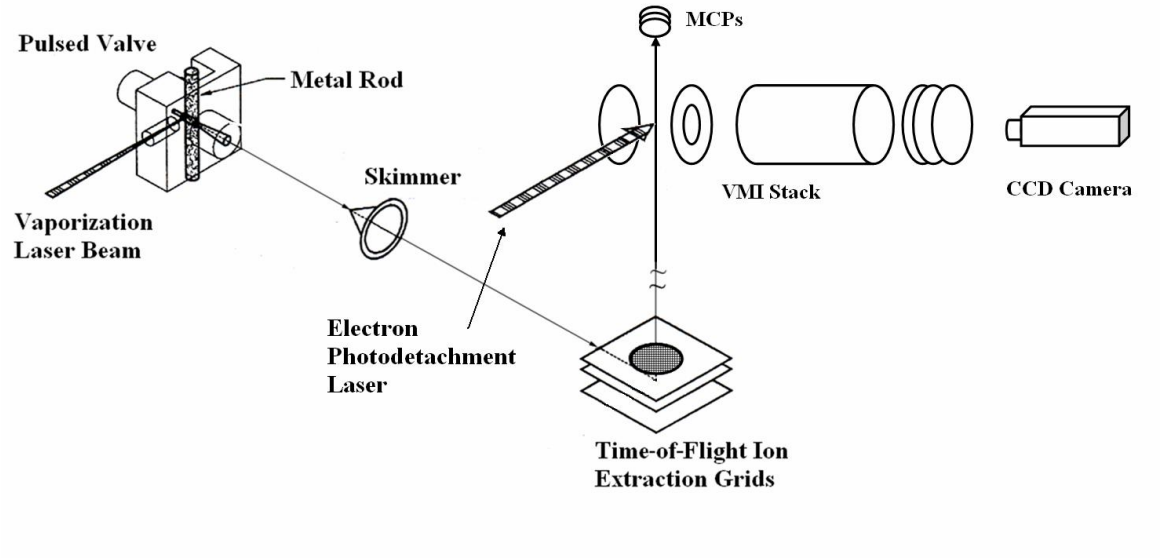

Figure **5.4**: Diagram of the instrument following addition of velocity map imaging (VMI) stack. A laser vaporization source is coupled to an anion time-of-flight mass spectrometer, which is equipped with a velocity map imaging apparatus.

3-D electron cloud. The BASEX software reconstructs the 3-D electron cloud image and removes a slice from the center. This slice is referred to as the reconstructed image and contains kinetic energy release information. The BASEX software is an improvement on previously used techniques to perform the inverse Abel transform, which were computationally expensive and produced noisy images.

The BASEX software also converts the reconstructed image to a speed distribution given as the number of photon counts verses pixel number. The pixel number is proportional to the kinetic energy of the photodetached electron. Subtracting kinetic energy from the known energy of the absorbed photon, the binding energy of the electron is obtained. For example, the known electron affinity of the copper anion is 1.236 eV; therefore, the kinetic energy of a photodetached electron is 1.094 following the absorption of one 532 (2.33 eV) photon. A plot of photon count vs. binding energy, as done in Figure **5.7**, results in the PES spectrum of Cu^-. The resolution of the instrument is determined by the peak's FWHM, which in this case is 105 meV.

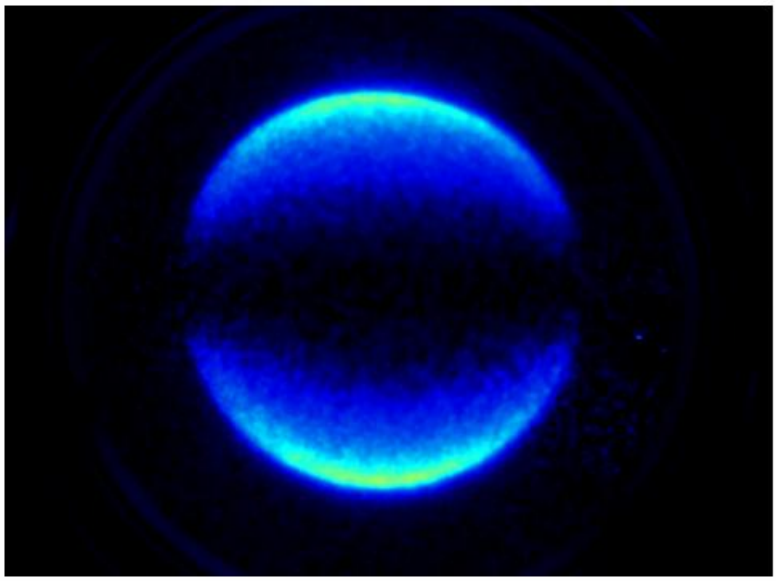

Figure **5.5**: Raw image of photodetached electrons from copper anions.

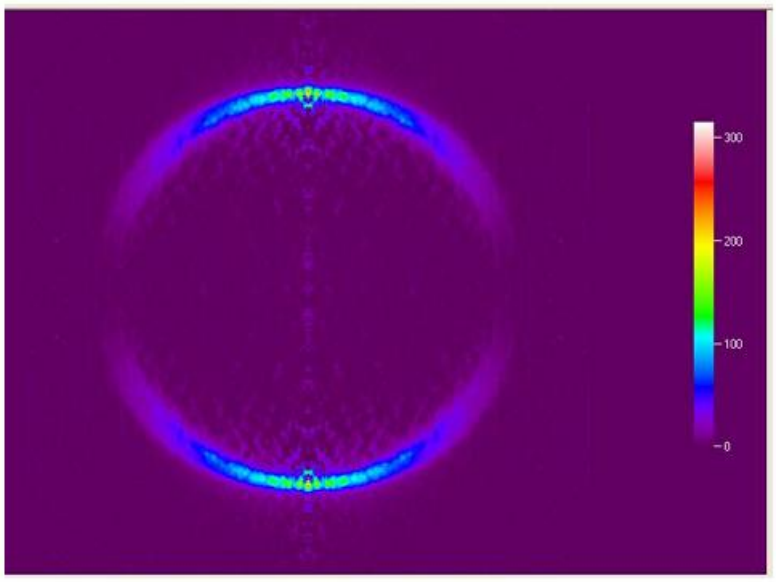

Figure **5.6**: Reconstructed image of photodetached electrons from copper anions using the BASEX Abel transform method.

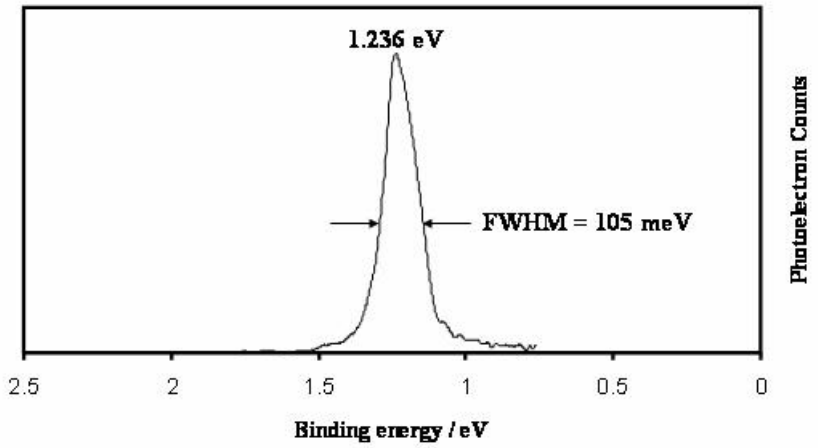

Figure **5.7**: Photoelectron spectrum of photodetached electrons from copper anions. The full width at half max (FWHM) is 105 meV.

5.4 References

1. A. J. R. Heck and D. W. Chandler, Annu. Rev. Phys. Chem. **46**, 335 (1995).

2. R. C. Bilodeau, M. Sheer, and H. K. Haugen, J. Phys. B **31**, 3885 (1998).

3. V. Dribinski, A. Ossadtchi, V. Mandelshtam and H. Reisler, Rev. Sci. Instrum. **73**, 2634 (2002).

Chapter 6

From Designer Clusters to Synthetic Nano-Crystals

The possibility of synthesizing nanoscale materials with clusters as their building blocks is one of the most promising prospects in the field of clusters and nanoscience.[**1**][**2**][**3**][**4**][**5**] These new materials would provide an unprecedented ability for synthesized customized materials, because the physical, chemical, electronic, optical, or magnetic properties of clusters are controllable by size and composition[**6**] The cluster materials, in addition, would possess intra-cluster and inter-cluster length scales, leading to novel functionalities not available in conventional solids.[**7**] While clusters are stable, the cluster materials are a meta-stable phase of matter and their compositions can not be predicted through conventional phase diagrams. The realization of this important concept therefore rests on the ability to identify stable motifs and processes that will enable the clusters to maintain their identity when assembled.

As pointed out by Castleman *et al.* [**8**], a new protocol is proposed in this chapter that provides a pathway to producing such materials more widely and with better control on primary units. The approach combines three major steps. (1) Identification of potential cluster species produced in molecular beams from bulk starting material. (2) First principles theoretical investigations, performed by Professor S. N. Khanna and his group members, to characterize electronic features and the bonding patterns that could guide the nature of assemblies and the conditions that might favor their formation. (3) Synthetic chemical approaches, accomplished by Professor A. Sen and his group

members, designed to facilitate the assemblies of desired cluster building blocks and eventually materials in bulk quantities. Through a synergistic effort combining the above steps, the feasibility of this procedure is demonstrated by making a solid via assembly and comprised of As_7K_3 units identified as being especially stable magic number species in the gas phase. An X-ray diffraction analysis of the synthesized material shows that the solid is characterized by As_7K_3 units that assemble into hexagonal rings. The hexagonal rings join together by sharing edges as in a graphite lattice and lead to a $(As_7K_{1.5})_\infty$ 3-D structure. The $K_{1.5}$ stoichiometry arises due to sharing of potassium by adjacent hexagonal rings in the extended structure; the remainder of the potassium is cryptated and occupies the cavities of the 3D-structure. The As_7 units exist in the As_7^{3-} state, and theoretical studies indeed confirm the stability of rings made out of As_7 and K units. The present example offers a viable protocol for accomplishing successful passage from free gas-phase clusters to cluster-crystals.

Elements belonging to group VA of the periodic table (N, P, As, Sb, and Bi), though similar in regard to the $ns^2\ np^3$ valence shells, exhibit a large variation in properties from the light to the heavy element. For example, N_2 has one of the highest homo-nuclear dissociation energies, i.e. 9.91 eV. The molecule is so stable that bigger units, e.g. N_4 would fragment into molecular units. On the other hand, As_2 has a modest dissociation energy of 4.17 eV and favors formation of larger units. For example, previous studies[**9**][**10**] have suggested that As_n (n=4, 8, 20, 32, 36, and 80) cages are quite stable and compound clusters composed of As cages have been synthesized. Note that while an As atom has a partially filled p sub-shell, bulk As is a semi metal. The variations in properties along with the existence of Zintl phases[**11**] suggest that it may be an ideal

system to explore the possibility of cluster based materials. The combination of As clusters with alkali atoms has also attracted considerable attention since some of the As clusters are stable in ionic form and the alkali atoms can provide the required charge. For example, As_5^- in As_5K is a very stable species due to the pi-bonding and aromaticity of the valence electrons.[**10**] Indeed, several Zintl phases composed of As and alkali metals clusters are known to exist.[**12**][**13**][**14**][**15**][**16**] Some involve As_7K_x as subunits in forming materials, but the protocol presented here for identifying the building blocks and approaching the assembly differs from others in that the gas phase cluster experiments are utilized to search for species that are stable and abundant magic numbers, which arise through self-assembly, and are thereby identified as viable building blocks for condensed phase nanoclusters of identical composition through assembly.

The gas-phase research described in following section is the contribution that I made to the research collaboration presented in this chapter. Section 6.2 explains theoretical efforts conducted by Dr. A. C. Reber, Dr. M. Qian and Professor S. N. Khanna, while Section 6.3 discusses synthetic research performed Dr. A. Ugrinov and Professor A. Sen.

6.1 Identification of stable cluster in gas phase experiments

The formation of a cluster solid requires motifs that will maintain their integrity upon assembly. The first step is then to investigate pure As, and As with alkali metals to identify any stable free species in the gas phase that may serve as building blocks. To accomplish this, the gas phase cluster techniques, discussed in Chapter 2 are implemented.[**17**][**18**] Specifically, As-K clusters were produced by vaporizing a

rotating and translating dispersed mixture of bulk arsenic and potassium, with the second harmonic (532 nm) of a Nd:YAG laser. The As-K target was created by mixing bulk potassium and arsenic, which was conducted inside a glove box to prevent oxidation of the potassium. Due to potassium being a soft metal, the mixture has the consistency of a paste. Then, a 1/4 inch section of a copper rod was turned down to 1/8 inch in diameter rather than its usual diameter of 1/4 inch, and the arsenic and potassium paste was placed within this void. While ablating the As-K target a cooling gas (methane seeded in helium) is pulsed into the region around the rod. The clusters form in a waiting room prior to supersonically expanding into a vacuum. The expansion is skimmed to form a pulsed molecular beam of As_xK_y clusters. The consequent pulsed neutral molecular beam of clusters is ionized with a XeCl excimer laser (308 nm), and then analyzed with a standard time-of-flight mass spectrometer.

Figure **6.1** shows the mass spectra of $As_nK_{3,4}^+$ clusters produced in this manner. A prominent cluster series, with compositions corresponding to known Zintl compounds, are readily formed. The clusters are comprised of As_n^{3-}, stabilized by three potassium atoms. Three such species are found with n=5,7,9; these are believed to be neutral clusters that are directly ionized in the analysis and associated detection scheme. Other members of the K_3 series, as well as clusters that contain four potassium atoms, may be stable cation fragments of larger arsenic and potassium clusters produced upon ionization. Note the prominent stability of the As_nK_3 cluster when compared to the other potassium containing compounds. The As_7K_3 is the most prominent "magic cluster" of the Zintl series which is identified as the building block for condensed phase materials as discussed below. Theoretical studies indicate that the ionization potentials of As_7K_3 and

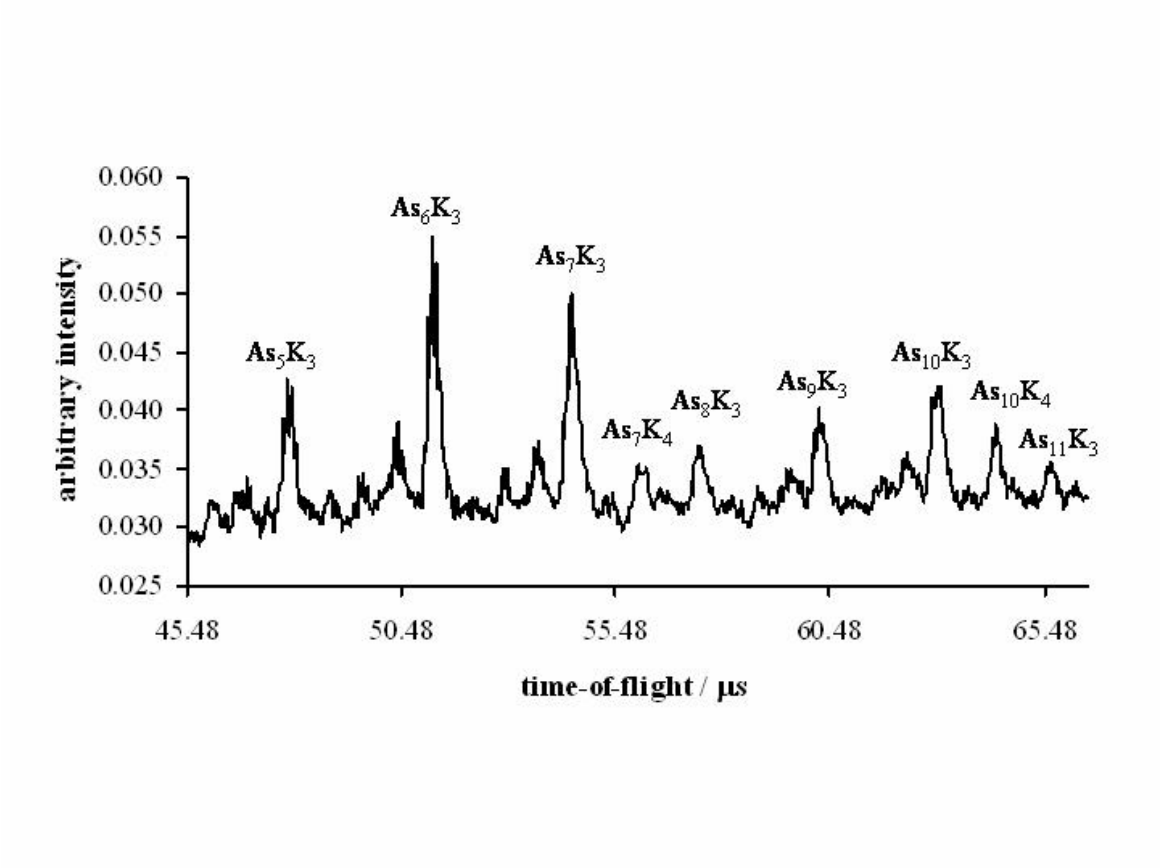

Figure **6.1**: Mass spectra of As_nK_m clusters generated in a molecular beam by the laser vaporization of a dispersed mixture of arsenic and potassium. Figure adapted from Castleman *et al.* [8].

other stable Zintl species are higher than the photon energy used to produce ionized species and hence involve a multiphoton process. On the other hand, the ionization potential of several other species and in particular that of As_6K_3 is less than the photon energy used for ionization. The $As_6K_3^+$, seen as the prominent peak in Figure **6.1** is either a product of a single photon ionization of the neutral or a stable fragment of the larger ionized species. In any event its positive charge prevents it, as well as any other stable cations, from serving as building blocks for condensed matter.

6.2 Energy landscapes to identify potential species

The observed stability of As_7K_3 and its viability for cluster assemblies were theoretically investigated through electronic structure studies by Professor S. N. Khanna and his group in collaboration. The stability of clusters was probed through two markers. First, removal energy (R.E.) defined as the energy needed to remove an As atom from a given cluster was calculated using the equation:

$$\text{R.E.} = E(As_{n-1}K_m)+E(As) - E(As_nK_m). \qquad (\mathbf{6.1})$$

Here $E(As_nK_m)$, $E(As_{n-1}K_m)$, and E(As) are, respectively, the total energies of a cluster containing n As and m K atoms, a cluster containing n-1 As and m K atoms, and an isolated As atom. The R.E. also represents the energy gain in adding an As atom to the preceding cluster. Peaks in plots of removal energy versus cluster size represent clusters where there is a larger gain in energy in forming the cluster from the preceding size, and smaller energy is required to form it by stripping an atom from the larger size. Both of these are indicative of a stable cluster. A similar R.E. can be defined for the growth

involving K atoms. The gap between the highest occupied molecular orbital and the lowest unoccupied molecular orbital (HOMO-LUMO) was used as the second marker. A relatively high HOMO-LUMO gap represents a cluster that is more chemically inert than other clusters.

In Figure **6.2** the R.E. and HOMO-LUMO gap for various clusters is displayed. In the case of pure As_n clusters (upper left insert), As_4 appears to be particularly stable due to its high R.E. and HOMO-LUMO gap, which corresponds well with other findings.[**10**][**19**] Another cluster that is marked by a high R.E and HOMO-LUMO gap is As_7K_3 (lower left pane). Hence, both experimental and theoretical findings point to As_7K_3 as being a promising candidate for developing cluster assembled materials.

Figure **6.3** shows the ground state geometry and the HOMO electronic charge density in the cluster. The K sites are seen to lose charge to the As_7 motif (Figure **6.3** (B)). A reasonable assignment of the cluster would be the arsenic motif tending towards anionic As_7^{-3} surrounded by K^+ cations. If the primary purpose of K is to donate charge, the stability of anionic As_7 could be looked upon from the following viewpoint. Assuming that each As contributes three valence electrons, an anionic As_7^{-3} unit would tend towards 24 electrons. The structure shown in Figure **6.3** has four sites with a coordination of three while three sites have double coordination. There are nine sigma bonds that are occupied by 18 valence electrons. In addition, the sites having double coordination with arsenic, form pi-bonds with the three base sites that are occupied by six electrons, which leads to a very stable structure. The next question is whether the As_7K_3 units will maintain their identity as the individual units are assembled to form cluster assemblies and eventually a

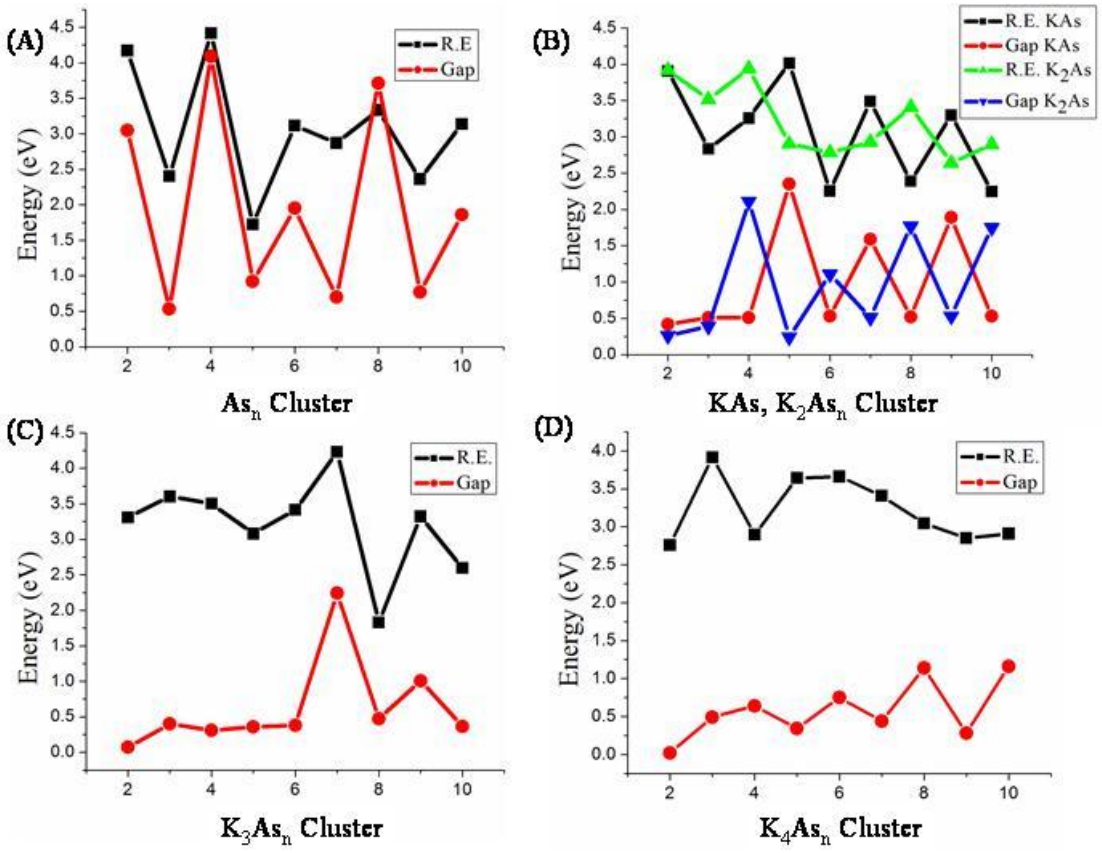

Figure **6.2**: Removal Energy (see Eq. (1)) and the HOMO-LUMO gap in the ground state structures of As_n, As_nK, As_nK_2, As_nK_3 and As_nK_4 clusters as a function of the number of As atoms. The energies are in electron volts (eV). Figure adapted from Castleman *et al.* [8].

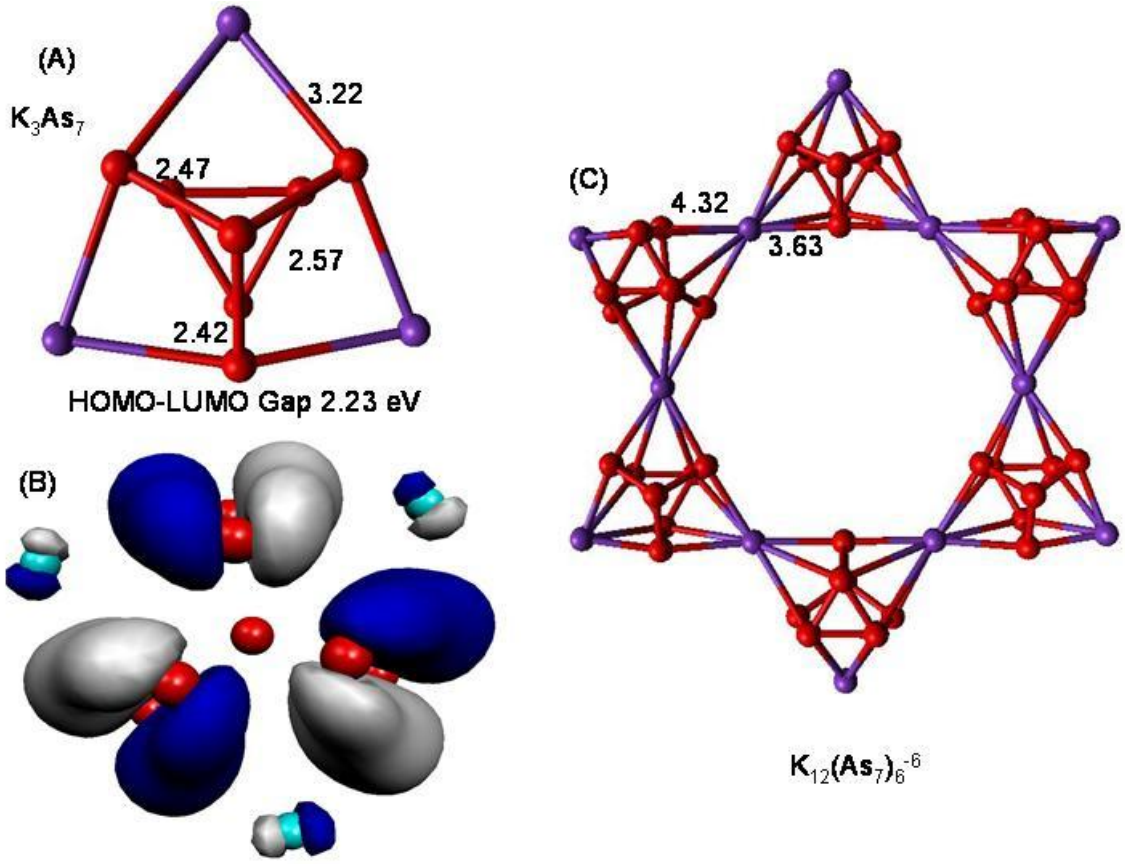

Figure **6.3**: (**A**) The ground state geometry of a K_3As_7 cluster (also marked is the HOMO-LUMO Gap). (**B**) The wave function in the HOMO of K_3As_7. (**C**) The optimized geometry of $K_{12}(As_7)_6^{6-}$ with no restraint. The charge from the additional 6 potassium atoms is compensated by the addition of 6 electrons. Figure adapted from Castleman *et al.* [8].

cluster-solid. To examine this possibility, Professor S. N. Khanna and his group calculated the ground state geometries of $(As_7K_3)_n$ super-clusters containing up to six basic units (See Figure **6.3 (**C)). In all cases, the individual As_7 units maintained their identity.

6.3 Synthesis and characterization of cluster-assembled material

The central issue is whether the stability in free beams and the theoretical prediction of stable rings can be translated to the formation of material in the condensed phase. To this end, a synthetic approach performed by Professor A. Sen and his group that relies on an assembly of clusters in solution was employed. More specifically, K, As, and $Ph_3SnCH_2SnPh_3$ (3:6:1 by weight) were mixed in ethylenediamine. The mixture was stirred overnight at room temperature and the resulting dark-green solution was filtrated. Crypt-222 (4,7,13,16,21,24-hexaoxa-1,10-diazabicyclo-[8.8.8]-hexacosane) (1:3 ratio versus K) was added to the solution, and it was layered with toluene. Orange crystals were formed on the wall and on the bottom of the test tube. Mother liquor was decanted and a crystal was used for single crystal X-ray diffraction.

X-ray diffraction data were collected from one crystal. The anionic species, As_7^{3-} (see Figure **6.4** (A), (B)) joined via K atoms, form an infinite 3-D structure with very high symmetry and with stoichiometry of $As_7K_{1.5}$. The arsenic cluster is very similar to the reported Zintl anion, As_7^{3-} (see Figure **6.4 (**C)).[15] Arsenic clusters and potassium atoms (Figure **6.4** (A)) form hexagonal rings which include six Zintl anions and six K

atoms (Figure **6.4** (A)). The hexagonal rings join together by sharing K atoms and form a three dimensional network.

As discussed above, the 3D framework has a negative charge, $(As_7K_{1.5})_\infty^{-1.5}$. The remaining potassium cations, those necessary to form a neutral compound and not included in the 3D-network, are cryptated and located within the cavity of the 3D-network. The formation of the network requires naked potassium ions but cryptated potassium ions are necessary for the integrity of the crystals.

The stability of rings containing six As_7 units linked by K raises the question: whether an isolated cluster with same overall charge would be stable. To this end, calculations on a free super-cluster composed of six As_7 units and 12 K atoms similar to those in the solid were performed. To incorporate the effect of cryptated K atoms in the solid, the resulting super-cluster was studied with a net charge of -6 (compensating for the missing potassium atoms). The ground state geometry is displayed in Figure **6.3** (C). One must point out that the calculations are on a single ring while the experiments are on a bulk solid. Significantly, the As_7K_3 is the prominent Zintl species found in the gas phase experiments.

6.4 Conclusions and future prospects

In summary, the results presented here demonstrate the development of a successful protocol for the production of nanoscale materials through cluster assembly. It involves the synergistic integration of three very different facets of cluster science: first, examining the stability of isolated gas-phase clusters in an interaction-free environment;

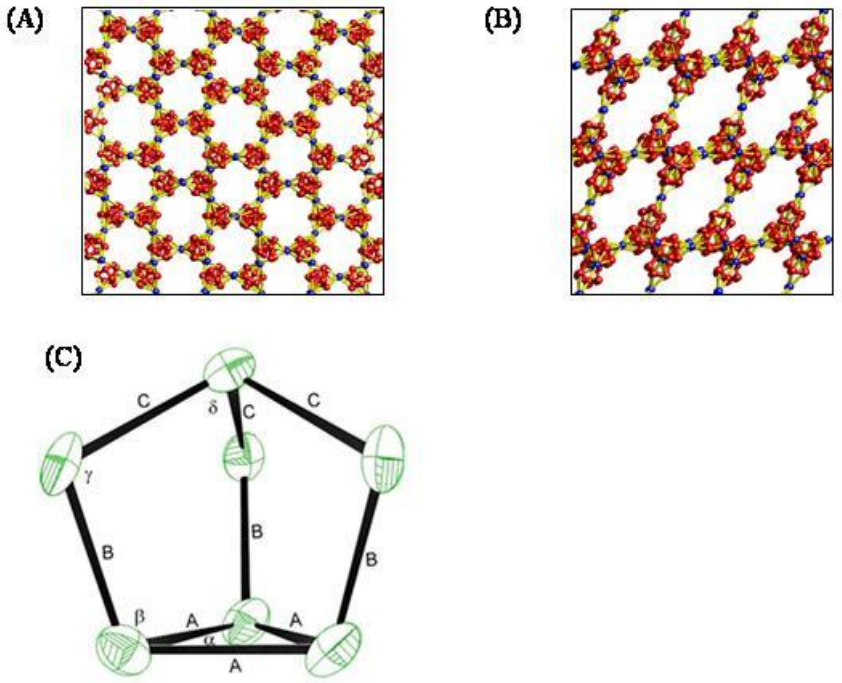

Figure **6.4**: Representation of the 3D-structure along: (A) the diagonal between a and b axes and (B) c axis (red – As-clusters, blue - K-atoms, yellow – bonds between the clusters and K-atoms). The cryptated potassium ions are located within the cavity of the 3D-network and are not shown for clarity. (C) The As_7^{3-} cluster, 50% thermal ellipsoids are used. Figure adapted from Castleman *et al.* [8].

second, carrying out theoretical investigations to identify the nature of bonding leading to the stability; and third, chemically synthesizing and structurally elucidating these cluster assemblies in the solid state. It has been shown that the passage from stable clusters in molecular beams to cluster assemblies involves going far beyond the conventional wisdom of merely focusing on a single magic peak seen in an experimental mass spectrum. On the contrary, major and minor peaks all need to be examined. In order to be an effective building block for new materials, the cluster has to be singularly stable towards variations in the composition of all the constituents, exhibit a large HOMO-LUMO gap, and have a geometry that will favor three dimensional assembly. The cluster charge and the use of sequestering agents (such as crypt-222) also play a role in separating the stable clusters during assembly.

6.5 References

1. S. N. Khanna and P. Jena, Chem. Phys. Lett. **219**, 479-483 (1994).

2. D. E. Bergeron, A. W. Castleman, Jr., T. Morisato and S. N. Khanna, Science **304**, 84-87 (2004).

3. D. E. Bergeron, P. J. Roach, A. W. Castleman, Jr., N. O. Jones and S. N. Khanna, Science **307**, 231-235 (2005).

4. J. Zhao and R.-H. Xie, Phys. Rev. B **68**, 035401 (2003).

5. W. Zheng, J. M. Nilles, D. Radisic and K. H. Bowen, J. Chem. Phys. **122**, 071101 (2005).

6. *Cluster Assembled Materials*, edited by K. Sattler (Trans Tech. Publications, Switzerland, 1996).

7. A. F. Hebard, M. J. Rosseinsky, R. C. Haddon, D. W. Murphy, S. H. Glarum, T. T. M. Palstra, A. P. Ramirez and A. R. Kortan, Nature **350**, 600-601 (1991).

8. A. W. Castleman, Jr., S. N. Khanna, A. Sen, A. C. Reber, M. Qian, K. M. Davis, S. J. Peppernick, A. Ugrinov, and M. D. Merritt, Nano Letters (submitted 2006).

9. T. Baruah, M. R. Pederson, R. J. Zope and M. R. Beltran, Chem. Phys. Lett. **387**, 476 (2004).

10. M. Shen and H. F. Schaefer, III, J. Chem. Phys. **101,** 2261-2266 (1994).

11. *Chemistry, structure, and bonding of Zintl phases and ions*, edited by S. M. Kauzlarich (VCH, New York, 1996).

12. J. D. Corbett, Chem. Rev. **85**, 383 (1985).

13. F. Emmerling and C. Rohr, Zeitschrift fuer Naturforschung, B: Chemical Sciences **57,** 963 (2002).

14. F. Gascoin and S. C. Sevov, J. Sol. State Chem. **175**, 306 (2003).

15. W. Schmettow and H. G. von Schnering, Angew. Chem. Int. Ed. Engl. **16**, 857 (1977).

16. T. Hanauer, M. Grothe, M. Reil and N. Korber, Hel. Chim. Acta **88**, 950 (2005).

17. R. W. Farley and A. W. Castleman, Jr., J. Am. Chem. Soc. **111,** 2735 (1989).

18. K. M. Davis, S. J. Peppernick, and A. W. Castleman, Jr., J. Chem. Phys. **124**, 164304 (2006).

19. W. Xu and B. Jin, J. Mol. Str.:Theochem **759**, 101-107 (2006).

Appendix A

Delayed Ionization of Niobium-Carbon Clusters

The purpose of this appendix is to discuss some interesting observations that were made while performing delayed ionization experiments on niobium-carbon clusters. The difference between the experiments conducted on niobium-carbon clusters in this appendix and the mixed metal carbon clusters studied in Chapter 3 is that a niobium rod was used in the laser ablation source rather than a mixed metal rod. The niobium carbon clusters are expanded into a vacuum and excited with 308 nm photons from an XeCl excimer laser. Normally, an electric field is used to direct ionized species down a field-free time-of-flight mass spectrometer. However, when studying delayed ionization, a reverse electric field directs ions away from time-of-flight mass spectrometer (TOF-MS) until time, *t*. Ions formed prior to *t* do not appear in the mass spectrum, whereas, species that ionize after *t* are detected by the TOF-MS. Figure **A.1** shows a delayed ionization experiment conducted on Nb_xC_Y where initially *t* is prior to the laser excitation of the clusters and prompt and delayed ions are detected. Then, *t* is stepped forward in time in 50 ns increments, which causes the detection of ions created at later and later times. The experiment is complete when no more ions are detected. The interesting observations that have been made regarding the delayed ionization experiments on niobium-carbon cluster are two-fold. First, the even-odd intensity change between the Nb_4C_x, Nb_5C_x, and Nb_6C_x, irregardless of the number of carbon atoms, is remarkable. In TOF-MS intensity

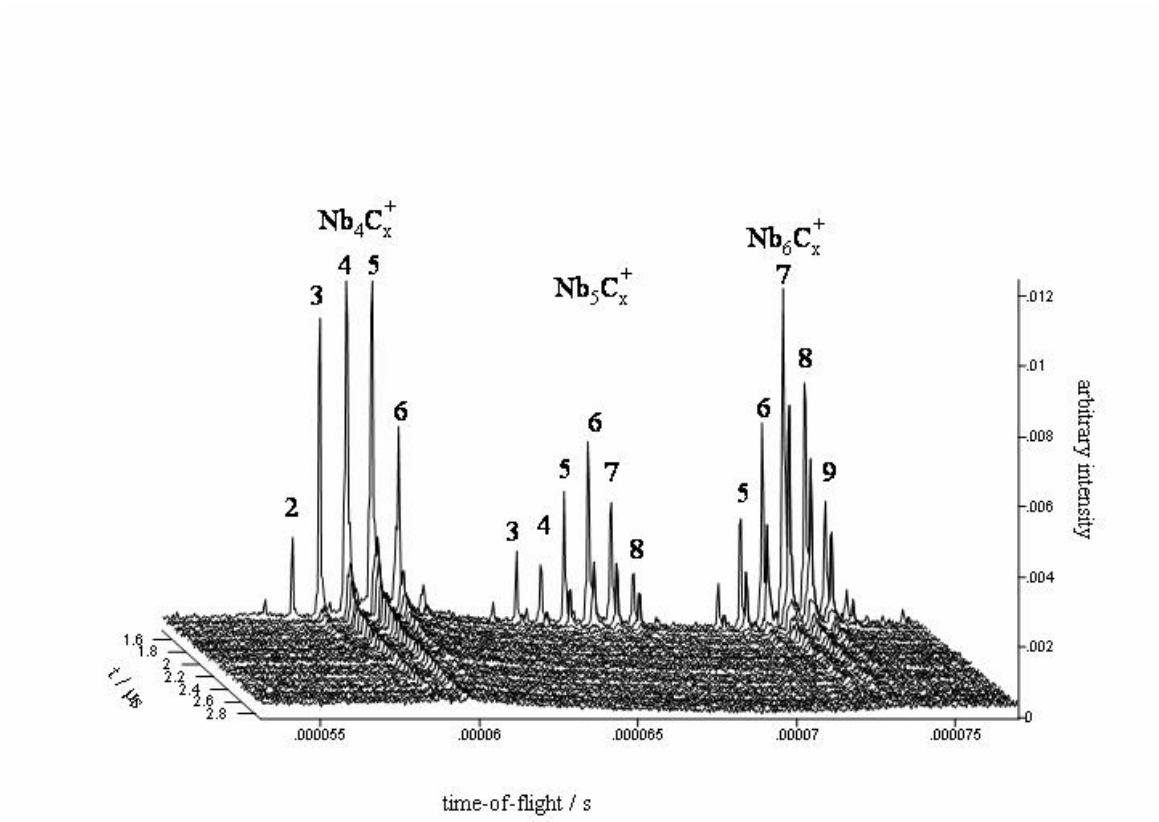

Figure **A.1**: Delayed ionization study of niobium-carbon clusters. Each mass spectrum represents the clusters that are in the acceleration region when the potential on the time-of-flight grid furthest from the detector (TOF 1) is pulsed to 4500 volts by a fast high voltage switch (FHVS) and therefore accelerated toward the detector. The electric field in the ionization region prior to the pulsing of the electric field is one that accelerates ions away from the detector. The timing (t) of the pulse from the FHVS is stepped forward in time in 50 ns steps until no further ions are detected. Time zero is the time at which the potential on TOF 1 is pulsed to 4500 volts and the ionization laser interacts with the molecular beam simultaneously. Spectra prior to time zero represent experiments wherein the potential on TOF 1 is pulsed to 4500 volts prior to the ionization laser interacting with the molecular beam.

often equates to stability of the cluster. Stable species form more abundantly in the cluster source. An even-odd trend in the intensity of noble metal clusters (M_n, where M is copper, silver and gold) has been reported in the literature.[**1**] The cause of this trend is attributed to M_n clusters, where n is even, have closed valence electron shells, because the noble metals have a filled d orbital and one electron in their valence s electron shell. Interestingly, niobium is another rare transition metal that has one electron in its valence shell. Its electron configuration is [Kr] $4d^4 5s^1$. Furthermore, if this even-odd trend of intensity was identified in pure niobium clusters, the trend seen in noble metal clusters might extend to niobium clusters as well. However, based on previous theoretical calculations,[**2**] it appears that niobium carbon clusters have very little niobium-niobium interaction, which would negate the shell closing hypothesis. Niobium-carbon clusters are thought to bond in a rock salt structure where niobium atoms are bonded to carbon atoms. Professor S. N. Khanna is performing theoretical calculations to better understand the level of niobium-niobium interaction in the niobium carbon clusters as well as investigate any other leads that may arise upon inspection of the theoretical results.

The second interesting observation lies in the same Nb_4C_x, Nb_5C_x, and Nb_6C_x cluster series. Note that the Nb_5C_x clusters show no sign of delayed ionization. Regardless of the low intensity of the Nb_5C_x, it is still interesting that there is no delayed ionization present. The $Nb_{4,6}C_x$ clusters show a 60-70% drop in intensity when comparing the prompt ions to the delayed ions. Therefore, if the Nb_5C_x clusters had the same percentage drop from prompt to delayed ionized clusters, delayed Nb_5C_x it would be detectable in the current experiment. The percentage of clusters that undergo delayed ionization is often determined by ionization potential, cluster stability, or photon

absorption cross-section. The two interesting observations may be linked, or they may have explanations that differ from one another. Again, inspecting previous theoretical investigations[**2**] on the niobium-carbon clusters of interest do not lead to any conclusions; however, the theoretical investigations are incomplete, and our collaboration with Professor S. N. Khanna hopes to be conclusive.

A.1 References

1. W. A. de Heer, Rev. Mod. Phys. **65**, 611 (1993).

2. H. Harris and I. Dance, J. Phys. Chem. A **105**, 3340 (2001).

VITA

Kevin Matthew Davis

Education

Doctor of Philosophy Degree, Chemistry (Mfay 2007)
The Pennsylvania State University (University Park)
Thesis title: "An Investigation of the Photoexcitation Dynamics and Stability of Clusters"
Advisor: Professor A. W. Castleman, Jr.

Bachelor of Science Degrees, Chemistry and Mathematics (May 2001)
Newman University (Wichita, KS)
Cum Laude

Honors

2005 Graduate Student Scholarship, *given by the Western Spectroscopy Association to outstanding graduate students who wish to attend the WSA annual conference*

2005 Graduate Student Travel Award, *given by the Eberly College of Science to graduate students with exceptional research accomplishments that wish to travel to a conference*

2004 Apple Fellowship, *given by the Eberly College of Science to graduate students with outstanding research accomplishments*

2004 Geiger Fellowship, *given by the Eberly College of Science to graduate students with outstanding research accomplishments*

2001 Roberts Fellowship, *given by the Eberly College of Science to excellent graduate school applicants*

Affiliations

American Chemical Society
American Physical Society
American Association for the Advancement of Science

Publications

"From Clusters to Crystals" A. W. Castleman, Jr., S. N. Khanna, A. Sen, A. C. Reber, M. Qian, **K. M. Davis,** S. J. Peppernick, A. Ugrinov and M. D. Merritt, *Nanoletters, submitted* (2006).

"Metal-carbon clusters: the origin of the delayed atomic ion" **K. M. Davis,** S. J. Peppernick, and A. W. Castleman, Jr., *J. Chem. Phys.,* **124,** 164304 (2006).

"Time resolved fluence studies and delayed ionization of the niobium-carbon cluster system" J. R. Stairs, S. J. Peppernick, **K. M. Davis,** and A. W. Castleman, Jr. *Israeli J. Chem.* **44,** 1-3 (Jortner part b) (2004).

"Delayed ionization of the zirconium Met-Car, Zr_8C_{12}" J. R. Stairs, **K. M. Davis,** S. J. Peppernick, and A. W. Castleman, Jr. *J. Chem. Phys.* **119,** 7857-7863 (2003).

"Metastable dissociation of the zirconium Met-Cars, Zr_8C_{12}, and connections to the production of the delayed atomic ion" J. R. Stairs, **K. M. Davis,** and A. W. Castleman, Jr. *J. Chem. Phys.* **117,** 4371-4375 (2002).

"Fundamental cluster studies of materials and atmospheric chemistry" D. P. Hydutsky, D. E. Bergeron, T. E. Dermota, J. R. Stairs, K. L. Knappenberger, Jr., **K. M Davis,** C. E. Jones, Jr., M.A. Sobhy, N. J. Bianco, S. J. Peppernick, And A. W. Castleman, Jr. *ISCANA Proceedings.*